

Linköping Studies in Science and Technology
Licentiate Thesis No. 1451

Controlling the Pore Size and Morphology of Mesoporous Silica

Emma M. Johansson



Linköping University

LIU-TEK-LIC-2010:22
Nanostructured Materials Division
Department of Physics, Chemistry and Biology (IFM)
Linköping University
SE-581 83 Linköpings Universitet, Sweden

© Emma Johansson 2010

ISBN: 978-91-7393-305-6

ISSN: 0280-7971

Printed by LiU-tryck
Linköping, Sweden, 2010

ABSTRACT

Mesoporous silica with a hexagonally ordered pore structure (SBA-15) has been synthesized. Through variations in the synthesis conditions several morphologies, such as fibers, sheets and separate rods, have been realized. Furthermore, additions of heptane and NH_4F make it possible to synthesize SBA-15 with pores as large as 18 nm in the sheet morphology. Mechanisms for the formation of different morphologies have been suggested. In the case of fibers and sheets, the amount of heptane present during the synthesis determines the final morphology. For low concentrations, the heptane enters the micelles and increases the pore size while the particles (crystallites) attaches to each other end to end. When the heptane concentration increases, the heptane droplets increase in size, and above a critical droplet size the crystallites attach with one short end towards the droplet, forming the sheet morphology. The crystallites can also be separated. This is the case of the rod morphology. The separation is performed by shortening the stirring time and increasing the HCl concentration. The increased amount of HCl increases the hydration rate of the silica precursor, which can be used to control the thickness and length of the rods. Furthermore, the reaction time has been decreased from 20 h for all morphologies to less than 4 hours. The materials have been characterized with nitrogen sorption, electron microscopy and x-ray diffraction. Also, thermogravimetric analysis and fourier transformed infrared spectroscopy have been used for studying the removal of surfactants.

PREFACE

This Licentiate Thesis is a part of my Ph.D. studies carried out in the Nanostructured Materials Division at Linköping University since June 2008. The aim of my research is in the first step to control the synthesis of mesoporous silica, gaining desired properties such as pore size and particle morphology and in the next step use it for different energy applications. The results are presented in the three appended papers. The research is financially supported by the Swedish Research Council (VR).

INCLUDED PAPERS

Paper I

Synthesis and characterization of large mesoporous silica SBA-15 sheets with ordered accessible 18 nm pores

E. M. Johansson, J. M. Córdoba and M. Odén

Materials Letters 63 (2009) 2129-2131

Paper II

Effect of heptane addition on pore size and particle morphology of mesoporous silica SBA-15

E. M. Johansson, J. M. Córdoba and M. Odén

Microporous and Mesoporous Materials 133 (2010) 66-74

Paper III

Rapid synthesis of SBA-15 rods with variable lengths, widths and tuneable 11- 17 nm sized pores

E. M. Johansson, M. A. Ballem, J. M. Córdoba and M. Odén

In manuscript

PAPERS NOT INCLUDED IN THE THESIS

Copper nanoparticles synthesized via electroless copper deposition in sheet-like mesoporous type SBA-15

H.-T. Tsai, J. M. Córdoba, E. M. Johansson, M. A. Ballem and M. Odén

Journal of Nanoscience and Nanotechnology (2010) DOI: 10.1166/jnn.2010.3609

Annealing of thermally sprayed Ti₂AlC coatings

J. Frodelius, E. M. Johansson, J. M. Córdoba, M. Odén, P. Eklund and L. Hultman

Accepted for publication in International Journal of Applied Ceramic Technology

ACKNOWLEDGEMENTS

There are many people I would like to thank for being a part of this work.

- First of all, my supervisor *Magnus Odén* for giving me (almost) free hands to explore the nature of mesoporous materials. For listening, encouraging, keeping me in the moment, good discussions and endless patience.
- My co-supervisor *José Córdoba* for help and support. For inspirational discussions and supervising me in how not to blow up the lab.
- All you guys in the lab during the years, *Mohamed, Jeffery* and *Klara*. For all great chats, discussions, extra hands and making life easier.
- *Mika Lindén* and *Jessica Rosenholm* at Åbo Akademi for XRD measurements and inspiring discussions.
- *Friends and co-workers at IFM* (you know who you are) for all your help and support. For all your input and ideas, great times and coffee breaks, game and movie nights and parties. You make me look forward to every day.
- *My family* for your love and support. For listening and encouraging me, even when you think I'm not living in the real world.
- Finally, *Jonas* for always being on my side supporting me in life. For love and patience.

TABLE OF CONTENTS

1	INTRODUCTION	1
1.1	Mold clay to form a bowl	1
1.2	It is the empty space that makes the bowl useful	1
1.3	Aim of the thesis	2
2	MESOPOROUS MATERIALS	3
2.1	Mesoporous silica	4
2.2	SBA-15.....	5
2.3	Applications	6
3	COLLOID AND SOL-GEL CHEMISTRY	7
3.1	Surfactants	7
3.2	Non-ionic triblock copolymers, Pluronics	8
3.3	Micelle formation with Pluronics.....	10
3.4	Silica precursor	14
4	SBA-15 SYNTHESIS	17
4.1	Formation	17
4.2	Hydrothermal treatment	18
4.3	Removal of surfactants	20
5	TUNING THE PROPERTIES OF SBA-15	23
5.1	Pore size	23
5.2	Wall thickness and microporosity	26
5.3	Morphology	28
5.4	Alkanes and NH ₄ F in a low temperature synthesis	32
5.5	Films	33
6	ANALYSIS TECHNIQUES	37
6.1	Physisorption	37
6.2	X-Ray Diffraction	45

6.3 Electron Microscopy	46
6.4 Thermogravimetric Analysis	48
6.5 Fourier Transformed Infrared Spectroscopy	49
7 SUMMARY OF RESULTS	51
7.1 Paper I	51
7.2 Paper II	51
7.3 Paper III.....	52
8 CONCLUSIONS	55
9 REFERENCES	57
PAPERS I-III	

I INTRODUCTION

“Mold clay to form a bowl. It is the empty space which makes the bowl useful.”

Lao Tzu

In my opinion, this old Chinese proverb expresses the essence in working with porous materials. We can shape them, make pores in varying sizes and structures and finally use all the surface and empty space in them for multiple applications.

Materials with large surface area have applications such as matrixes for catalysts, chemical reactors and gas storage. To increase the surface area of a material, the particle size of the material can be reduced or open pores can be introduced. In this thesis highly porous silica will be studied.

1.1 Mold clay to form a bowl

Mesoporous materials have pores in the size range of 2 to 50 nm. It is common to use two different paths for syntheses of materials on the nanoscale: top-down or bottom-up. In the top-down approach one starts from the top, from a larger unit, and shape this unit into a nanostructure by for example cutting or milling. The top-down approach is used for manufacturing e.g. microchips and micro-patterning. The bottom-up approach is based on properties of single molecules which can self-assemble and form structures. This approach is common when mesoporous materials are synthesized by self-assembly of surfactants to form micelles and condensation of metal species onto these micelles. Variations in the final material such as different pore sizes and morphologies can be gained by changing the properties of the original molecule.

1.2 It is the empty space that makes the bowl useful

Materials with high open porosity have a large available surface area compared to materials with no or closed porosity, see Figure 1. In mesoporous silica the specific surface area is commonly 500-1000 m²/g which is approximately the area of a handball court in the volume of a water glass. The high specific surface area

of mesoporous silica makes it an excellent substrate for catalysts and mesoreactors where chemical reactions take place in the pores.

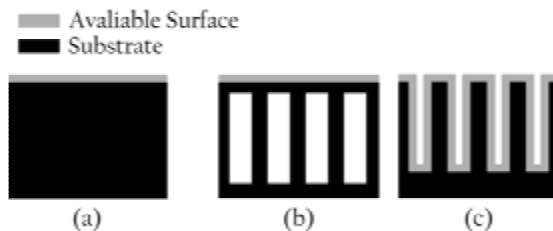


Figure 1. Available surface in (a) solids and materials with (b) closed and (c) open porosity.

The narrow pore size distribution of mesoporous silica also makes it suitable as templates for other materials and as a constrainer when growing nanoparticles inside the pores.

1.3 Aim of the thesis

In this thesis the synthesis, characterization and application of mesoporous silica SBA-15 with unusually large pores (≤ 18 nm) is presented. The material consists of ~ 400 nm crystallites with cylindrical, hexagonally ordered pores running through them. The crystallites are either monodispersed or attached to each other, forming different morphologies such as fibers or sheets. If instead the crystallites are attached to a substrate, a porous film is formed in which the pores can be oriented parallel or perpendicular to the substrate. The monodispersed crystallites can be elongated and thereby the thickness of the mesoporous film is controlled.

This thesis will be the foundation of my future research as a Ph.D.-student where I will study applications for the material described in these papers.

2 MESOPOROUS MATERIALS

Mesoporous materials are materials with pores in the range of 2–50 nm according to the IUPAC classification in which

micropores have a diameter < 2 nm,

mesopores have a diameter between 2 and 50 nm and

macropores have a diameter > 50 nm [1].

The pores can have different shapes such as spherical or cylindrical and be arranged in varying structures, see Figure 2. Some structures have pores that are larger than 50 nm in one dimension, see e.g. the two first structures in Figure 2, but there the width of the pore is in the mesorange and the material is still considered to be mesoporous.

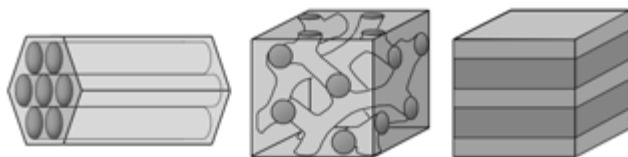


Figure 2. Different pore structures of mesoporous materials.

Mesoporous materials can have a wide range of compositions but mainly consists of oxides such as SiO_2 , TiO_2 , ZnO_2 , Fe_2O_3 or combinations of metal oxides, but also mesoporous carbon can be synthesized [2-6]. Most commonly is to use a micellar solution and grow oxide walls around the micelles. Both organic metal precursors such as alkoxides [7-9] as well as inorganic salts such as metal chloride salts [3] can be used. Alternatively a mesoporous template can be used to grow another type of mesoporous material inside it. This is often used for synthesizing e.g. mesoporous carbon [6,10,11].

2.1 Mesoporous silica

In 1992 a new family of ordered mesoporous materials was reported [2,7] and this became the starting point of a new research field. These materials are named MCM- X (Mobil Crystalline of Materials) and were synthesized by Mobile Corporation laboratories. Mesoporous silica with different pore structures were synthesized e.g. MCM-41 with hexagonally ordered cylindrical pores and MCM-48 with a cubic pore structure. These materials are synthesized with cationic surfactants under basic conditions.

This was though not the first attempt of synthesizing mesoporous silica. There is a patent from 1971 regarding synthesis of low-density silica where cationic surfactants were used [12]. In this patent there is no report concerning porosity, only the low bulk density was of importance. Later this material has been synthesized, characterized and compared to MCM-41[13]. It is clear that this material is a predecessor to the mesoporous silica that is synthesized today, even though the importance of this type of material was not recognized then.

The first mesoporous silicas synthesized with non-ionic triblock polymers were reported in 1998 by Zhao et al. [8,14]. These materials are named SBA- X (Santa Barbara Amorphous) where X is a number corresponding to a specific pore structure and surfactant, e.g. SBA-15 has hexagonally ordered cylindrical pores synthesized with P123 as surfactant while SBA-16 has spherical pores arranged in a body centred cubic structure and is synthesized with F127. SBA-15 is the most extensively studied mesoporous silica and also the subject of attention in this thesis.

Other families of mesoporous silicas are e.g. MSU [15], KIT [16], FDU [17] and AMS [18] where the materials are synthesized with variations in e.g. synthesis conditions and surfactants.

2.2 SBA-15

SBA-15 is a mesoporous silica (SiO_2) which has cylindrical pores arranged in a hexagonal order synthesized with the Pluronic triblock-copolymer P123. The structure of SBA-15 is illustrated in Figure 3. For this material, the pore size refers to the width of the cylindrical pores which can be tuned between 4-26 nm [8,14,19,20] even though pore sizes above 12 nm are rare. The length of the pores varies from ~200 nm [21,22] to several microns.

Around each mesopore is a microporous network called the corona [23,24]. This network interconnects the mesopores with each other and is responsible for the high surface area of SBA-15. The microporous network was first shown by platinum replicas [24] where the nanorods from filled mesopores were interconnected by the network which makes the nanorods remain in the hexagonal structure even after removal of the silica, see Figure 3.

The corona is mainly supposed to originate from trapped hydrophilic chains of the surfactants [25-27]. An additional explanation for the corona is stress-induced defects where the micropore fraction increases with the effective pore wall thickness to average pore diameter ratio [28]. It is stable up to 1173 K, but above this temperature the network disappears and the material has similar structure to MCM-41 [24].

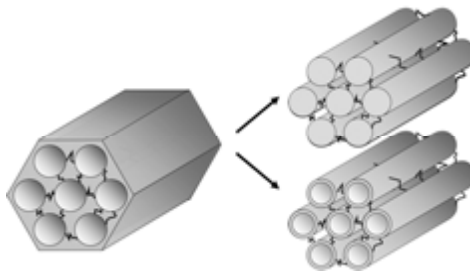


Figure 3. The structure of mesoporous silica SBA-15 (to the left) and its replica in form of rods (top right) and straws (down right).

The corona plays a crucial role when using SBA-15 as a template for other materials. Replicas can be synthesized in two variants, one rod-like and one straw-like see Figure 3. Due to that the micropores also will be filled with the replica material the mesopore replicas will be fixed in the hexagonal structure and the particle morphology will be retained. If instead MCM-41 is used as template, the end result is more similar to spillikin.

2.3 Applications

As mentioned earlier platinum replicas of SBA-15 has been synthesized, but the most common material for replicas of SBA-15 is carbon. These replicas can be formed either as rod-like or straw-like [5,6,29,30], see Figure 3. The replicas can then be used as new templates for other mesoporous materials [31], as supports for e.g. platinum particles [10] or as storage units for e.g. hydrogen or methane [32,33]. Replicas of SBA-15 can also be synthesized of metal oxides such as CeO_2 , Cr_3O_4 , MnO_2 or WO_3 , see [31] and references therein.

It is also possible to use SBA-15 as a template for growing nanoparticles or nanowires of pure metals or metal oxides [34,35]. The particles can then be removed from the silica matrix or the composite can be used in catalysis [36].

An alternative to nanoparticles in catalytic applications is anchoring of functional groups into the silica walls [36]. Alternatively, more reactive materials such as Ti can be incorporated in the silica walls during the synthesis to make the surface more reactive, e.g. incorporation of Ti makes the SBA-15 suitable for hydrogen storage and photovoltaic applications [37]. Functionalization of the surface also gives the opportunity to use SBA-15 e.g. as a carrier in drug delivery systems [38-41] or in storage of methanol [42].

Finally, the possibility to control the pore size of SBA-15, as well as the narrow pore size distribution, makes SBA-15 a good candidate as a molecular sieve for biomolecules [43] and it is useful in the separation of hydrocarbons [44].

3 COLLOID AND SOL-GEL CHEMISTRY

The synthesis of SBA-15 is called sol-gel synthesis. The solution (sol) is the colloidal system where micelles are formed by surfactants and are dispersed in an aqueous solution. When the silica precursor is added to the sol it hydrolyses and a silica network is formed in which the liquid is enclosed, a gel. The transition between sol and gel is gradual and the sol becomes a gel when it can support a stress elastically. Finally the gel is heated (calcinated) whereby the surfactants decompose and evaporates. Left is now the porous silica network.

3.1 Surfactants

Surfactants (surface active agents) are amphiphilic molecules, i.e. they are composed of a hydrophilic (water-loving), and a hydrophobic (water-hating), part, see Figure 4. Surfactants are classified by their head group: anionic, cationic, zwitterionic and non-ionic. The lipophilic part is often a hydrocarbon chain. Due to their amphiphilicity, the surfactants form micelles in oil or aqueous solutions to lower the free energy in the system. If the solvent have two immiscible phases the surfactants are located in the oil/water interface with the hydrophilic part towards the water and the lipophilic part in the oil.

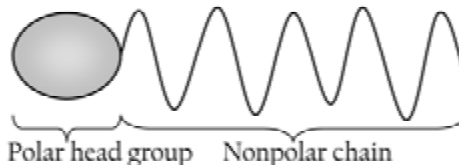


Figure 4. Schematic picture of a surfactant.

3.1.1 Micelle formation and structures

When the concentration of surfactants is low in an aqueous solution, the surfactants are located as separate molecules in the air/water interface. This reduces the surface tension since it is larger for water than for the hydrocarbons. Increasing the surfactant concentration in the solution further reduces the

surface energy until a critical value. At this point, the critical micelle concentration (CMC) is reached and aggregates of surfactants (micelles) are formed. The CMC is determined by two competing factors; bringing the nonpolar chains out of the water phase into the oil phase (hydrophobic effect) and repulsion between the polar head groups which opposes the formation of micelles [45]. The CMC and shape of the micelles are determined by the nature of the surfactant and conditions in the solution such as temperature or salt additions.

The aggregate structure of the amphiphilic molecules is determined by the critical packing parameter (CPP)

$$CPP = \frac{v}{l \cdot a} \quad (1)$$

where v is the volume of the hydrophobic chain [nm^3], a is the area of the hydrophilic part [nm^2] and l [nm] the length of the hydrophobic chain. The volume v and length l can be expressed by

$$v = 0.027(n_C + n_{Me}) \quad (2)$$

$$l = 0.15 + 0.27n_C \quad (3)$$

where n_C is the number of carbon atoms and n_{Me} the number of methyl groups. The relation between CPP and aggregate structure is illustrated in Figure 5. The cylindrical hexagonal micelles needed to form SBA-15 has $1/3 < CPP < 1/2$.

3.2 Non-ionic triblock copolymers, Pluronics

When mesoporous silica is synthesised, several types of surfactant can be used e.g. cationic CTAB [2,7], non-ionic PEO surfactants [15] or Pluronics [8]. In this work Pluronic P123, a non-ionic amphiphilic triblock copolymer, Figure 6, has been used as surfactant.

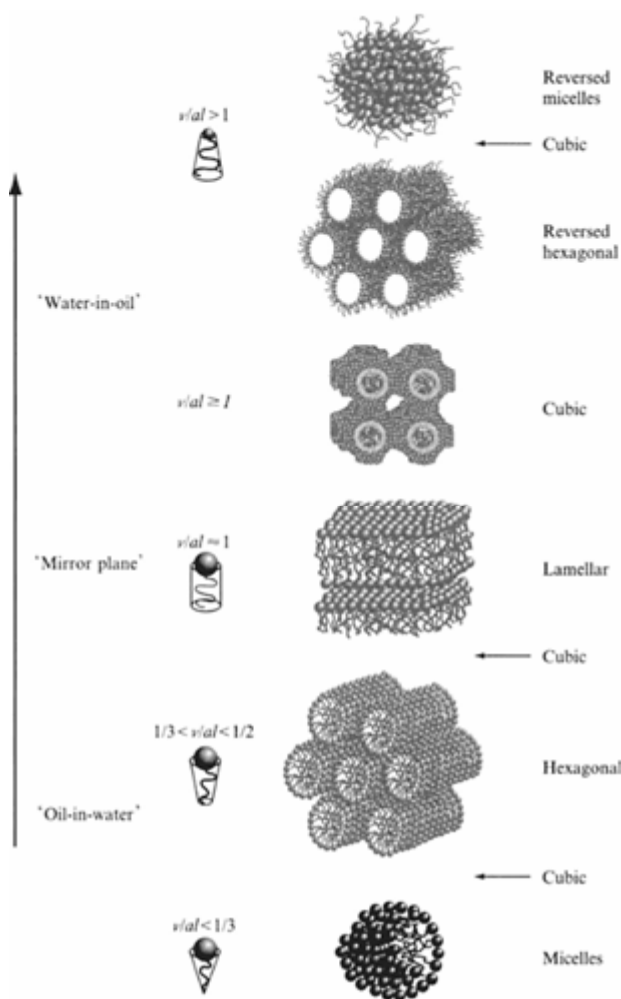


Figure 5. Critical packing parameters of surfactant molecules and preferred aggregate structures for geometrical packing reasons [46]. Reprinted with permission from John Wiley & Sons Ltd.

There are several non-ionic triblock copolymers under the trademark Pluronics. These polymers were patented in 1973 and are also called Poloxamers [47]. They all consist of hydrophilic polyethylene oxide chains (PEO) and hydrophobic polypropylene oxide chains (PPO). There are several different Pluronics with varying molecular weights and PEO/PPO ratios ($EO_xPO_yEO_x$). The notation for a

Pluronic triblock copolymer starts with a letter followed by two or three numbers. The letter describes the appearance of the polymer: F (flake), P (paste) or L (liquid). The first one or two numbers multiplied with 300 indicates the molecular weight of the PPO block and the last number gives the PEO weight fraction [48]. Hence, P123 is a paste with ~3 600 g/mol PPO and 30 wt% PEO while F127 is solid flakes with the same weight of PPO but 70 wt% PEO. These differences give rise to the variation of pore structures observed in the mesoporous materials, e.g. F127 is used for synthesizing spherical pores in a body centred cubic structure while P123 is used for hexagonally ordered cylindrical pores [8].

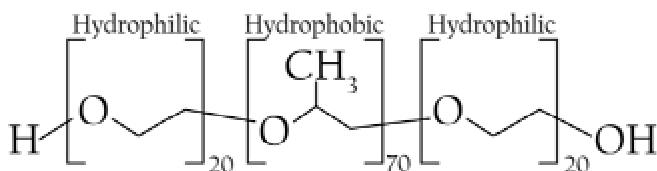


Figure 6. Chemical formula and properties of the surfactant P123.

3.3 Micelle formation with Pluronics

As mentioned earlier, the concentration of surfactants and temperature of the solvent is crucial for the formation of micelles. These two parameters vary for the PEO-PPO-PEO surfactants with respect to the structure and weight of the polymers. For example, Pluronics with PEO segments of the same size have both the CMC and critical micelle temperature (CMT) decreasing with increasing PPO size. The size effect of the PEO chain is less pronounced than the effect of the PPO size. It is clear that for Pluronics the micelle formation is driven by the PPO chain [49-51]. The micelles consist of a hydrophobic PPO core surrounded by hydrophilic PEO chains which form a corona around the core.

3.3.1 Temperature dependence

The properties of the PEO and PPO blocks are highly temperature dependant since the hydration of methyl groups in both blocks depends on the temperature [51,52].

During the micelle formation process there are three temperature regions of importance: the unimer region (where the surfactants are not aggregated), the transition region and the micelle region [53,54]. At low temperatures, the unimer region, the methyl groups of the PPO blocks becomes hydrated and can form hydrogen bonds with the water. When the temperature is increased the methyl groups rotate and the hydrogen bonds are broken [52,55]. At CMT and during the transition region there is a mixture between micelles and unimers. In this region the interaction between PPO and water is reduced and the PPO chains instead interact with each other. Thereby the micelles with nonpolar, hydrophobic cores are formed. This is happening gradually for a small temperature interval of ~ 10 °C [52,55]. Finally the micelle region is reached and all surfactants are aggregated to form micelles.

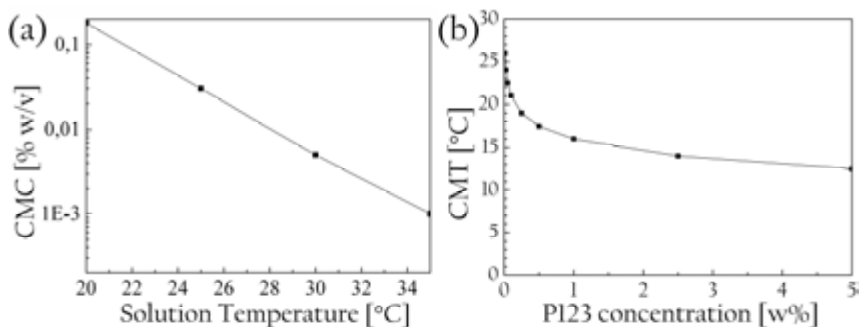


Figure 7. The relation between micelle concentration and solution temperature. Data from ref. [49].

The CMT depends on the concentration of micelles in the solution, see Figure 7 (b). This is of great importance when synthesising mesoporous materials. The CMT can be changed for a given surfactant concentration by adding salts. This will be discussed further in section 3.3.3.

Above CMT, spherical micelles increase in size with increasing temperature until the micellar core reaches the radius of a completely stretched PPO chain. At this point the structure of the micelles changes from spheres to cylinders [54]. A phase diagram is useful for finding CMC, CMT and micellar shapes, as seen in Figure 8.

Water becomes a worse solvent for the PPO and PEO chains when the temperature is increased due to the increasing number of polar states. Above a critical temperature, the cloud point (CP), the surfactants can no longer be dissolved to form micelles and instead they precipitate from the solution [56,57].

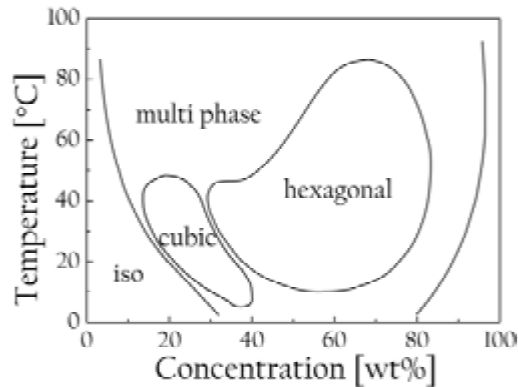


Figure 8. Phase diagram of P123 in water. After ref. [51].

3.3.2 Sphere-to-rod transition

To form the cylindrical pores in SBA-15 the micelles must undergo a transition from spherical to cylindrical shape. During the synthesis, the temperature and surfactant concentrations are kept constant. Hence, other parameters during the synthesis are responsible for this change in CPP leading to the sphere-to-rod transition.

During the synthesis, this transition occurs upon addition of the silica precursor, TEOS, which will be described in section 3.4. Ethanol is a decay product of TEOS, and in a given temperature range PPO is soluble in ethanol. When the ethanol goes into the hydrophobic core of the micelles, the core volume expands and the CPP increases according to Eq. (1) [58].

The transition can also occur upon additions of salt [59], or increasing the temperature [60] since these decrease the hydrophilic area of the surfactants due to dehydration of the PEO chains.

3.3.3 Salt additions

The addition of salt to the synthesis of SBA-15 makes it possible to decrease the synthesis temperature from 35 – 55 °C to as low as 10 °C [61-64], Smaller pore sizes are achieved when a combination of salt additions and a low temperature (and no swelling agents) are used.

The properties of non-ionic triblock copolymers, such as P123, are also strongly affected by salt additions. By salt additions CMT, the sphere-to-rod transition and CP can be shifted. The shifts are proportional to the concentration of salt. For example, F^- , Cl^- , Br^- , Na^+ , K^+ and Li^+ decreases the CMT, sphere-to-rod transition and CP while SCN^- increases the solubility of P123 that gives higher temperatures for the transitions. Anions have a larger effect on the CMC and CP than cations [50,65].

It has been shown that $CMT_{no\ salt} - CMT_{salt} = CP_{no\ salt} - CP_{salt}$ when salt are added to a solution except for I^- which instead increases CP and decreases CMT. This is very useful, since sometimes only one of these two parameters can be studied [65].

Most, but not all, salts decrease the solubility of organic polymers (salting out phenomena). Some salts act as structure makers for the water and increases the self-hydration of water through hydrogen-bonding. Other salts act as structure breakers and decrease the number of hydrogen-bonded OH groups [66]. Anions give a stronger effect on solubility of polymers and their salting out strength at a given molar concentration follows the Hofmeister series: $SO_4^{2-} \approx HPO_4^{2-} > F^- > Cl^- > Br^- > I^- > SCN^-$. Ions preceding Cl^- in the series are polar water-structure makers and those after Cl^- water-structure breakers. Cl^- has little effect on water structure [67].

It is commonly said that salts increase the solvophobicity of PEO and PPO chains and therefore induce micelle formations [57] and it is known that PEO chains form aggregates in water solutions with salt additions. It has been suggested that this aggregation is driven by the structuring of water [68]. The PEO chains are surrounded by a zone where water has increased structure [69]. When an ion approaches a PEO segment the amount of water between these two decreases. PEO is far less polarisable than water and the removal of the polarized water will

induce a repulsive force between the ion and PEO chains. On the other hand, the removal of water leads to an attractive force between the PEO chains. The total force from these two contributions depends on the ion. The larger the ion, the more attractive the force will become. This is due to that for larger ions, a larger amount of structured water will be expelled [65,70].

The effect of cations on the other hand, does not follow the Hofmeister series, but instead the effect depends on the counter ion [59]. This can be due to that there is not as large size difference between cations as for anions [70]. For Cl^- as anion the effectiveness of cations follow $\text{Cs}^+ \approx \text{K}^+ > \text{Li}^+$ [59].

3.4 Silica precursor

Several types of silica precursors can be used for mesoporous silica. The most common are alkoxides, especially tetramethyl orthosilicate (TMOS) or tetraethyl orthosilicate (TEOS), see Figure 9, but other alkoxides with longer alkyl chains can be used [71]. An alternative, cheaper, silica precursor that can be used is sodium silicate [72,73] or combinations of this and alkoxides [74]. In this work, only TEOS has been used as the silica source.

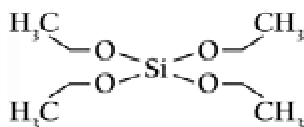


Figure 9. Chemical formula of the silica precursor TEOS.

In aqueous solutions the alkoxides hydrolyses (i) and polymerises to form a silica network (ii) and (iii). Both steps can be controlled by varying pH and adding salts to the aqueous solutions as described in literature reviews [75,76] and references therein.

- (i) Hydrolysis $\equiv \text{Si} - \text{OR} + \text{H}_2\text{O} \leftrightarrow \equiv \text{Si} - \text{OH} + \text{ROH}$
- (ii) Alcohol condensation $\equiv \text{Si} - \text{OR} + \text{HO} - \text{Si} \equiv \leftrightarrow \equiv \text{Si} - \text{O} - \text{Si} \equiv + \text{ROH}$
- (iii) Water condensation $\equiv \text{Si} - \text{OH} + \text{HO} - \text{Si} \equiv \leftrightarrow \equiv \text{Si} - \text{O} - \text{Si} \equiv + \text{H}_2\text{O}$

The hydrolysis of TEOS needs an acid or basic catalyst to occur, and the hydrolysis rate is directly proportional to the concentration of acid or base. In general, short alkyl chains hydrolyse faster than long chains. Hydrolysis and gelation occurs simultaneously. H_3O^+ increases the rate of hydrolysis while OH^- increases the gelation rate, so at pH suitable for synthesis of SBA-15 (pH \approx 2) the hydrolysis is fast but the polymerization is slow.

In the presence of alcohols, the hydrolysis rate of TEOS is reduced [77]. This can be used for controlling the morphologies of SBA-15.

4 SBA-15 SYNTHESIS

The synthesis of SBA-15 is straight forward and uncomplicated. First the surfactant, P123, is dissolved in hydrochloric acid and then the silica precursor, e.g. TEOS, is added. This solution is stirred for a given time (2-20 h) at 40 °C and then heated to 80-130 °C for 24-72 h (hydrothermal treatment). Finally the product is collected by filtration and calcinated at 550 °C to remove the template. There are several ways to control the pore size, microporosity and particle morphology to obtain the optimal product, e.g. addition of salt, swelling agents and/or temperature variations which will be discussed here.

4.1 Formation

The formation mechanism of SBA-15 is assumed to be similar to the formation of MCM-41 which was suggested by Beck et al. to be a liquid crystal mechanism [7]. This can be seen in Figure 10 and shows how the micelles starts as spherical and when the silica precursor is added, the micelles becomes elongated and arranges themselves in a hexagonal pattern while the silica walls are built. After calcination, the surfactants are removed and only the mesoporous silica remains.

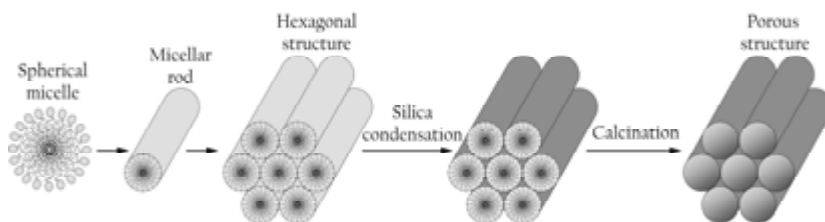


Figure 10. Illustration of the formation mechanism suggested by Beck et al. [7].

Experimental studies of the formation of SBA-15 with e.g. SAXS, NMR and TEM [78-80] have shown that when the silica source is hydrolyzed it is adsorbed on the PEO chains of the micelles. The polymerization of the silica introduces an attractive interaction between the micelles which leads to the formation of flocs of micelles. These domains grow larger and the final structure is reached. The

time for elongation of the micelles has been thoroughly discussed, if it occurs prior to or during the formation of flocs. SAXS and cryo-TEM have though shown the presence of separate threadlike (cylindrical) micelles prior to the floc formation [80,81].

The mechanism of the elongation of the micelles has been studied with various techniques [26,81,82]. Prior to the addition of silica precursors the micelles are spherical but TEOS and TMOS are hydrophobic, so when they are added to the synthesis they enter the hydrophobic core of the micelles. The hydrolyzed precursors then diffuse into the corona region and adsorb onto the P123 and the polymerization process begins in the core/corona interface and continues then only in the corona. The polymerization in the core/corona region is simultaneous to the elongation of the micelles while the polymerization in the pure corona is associated with the precipitation of flocs. When the silica precursor is polymerized on the PEO chains, the water content in this area is decreased. This changes the polarity resulting in a reduced curvature of the micelle and hence, the micelles become elongated.

Theoretical modelling of the formation of mesoporous materials has shown that the silica preferably adsorbs onto low curvature sections of the micelles. During the elongation of the micelles the surface energy of the spherical caps on the ends increases and therefore no silica will attach there, leaving the pore ends open in the calcinated material [83].

4.2 Hydrothermal treatment

When the formation of SBA-15 is finished, the temperature is increased and the hydrothermal treatment begins. As mentioned in section 3.3.1 the properties of P123 is temperature dependent and therefore this is a good way of tuning the properties in term of pore size, micropore volume and surface area of the final product. Several studies of the effect of the hydrothermal treatment have been performed on standard syntheses [14,84-87], with varying silica precursors [73], and syntheses with swelling agents [88].

The effect of the hydrothermal treatment is twofold. First, after the formation of the hexagonal structure, the PEO chains are trapped into the silica network

[26,86] and they are the source for the micropores in the final product. When the temperature is elevated, the hydrophilicity of the PEO chains change and becomes more hydrophobic. The chains then retract from the silica wall and go into the more hydrophobic core of the micelles. The result of this is an increased pore size and reduced microporosity and surface area. Secondly, the hydrothermal treatment decreases the shrinkage of the silica walls upon calcination. The effect of hydrothermal treatment is illustrated in Figure 11.

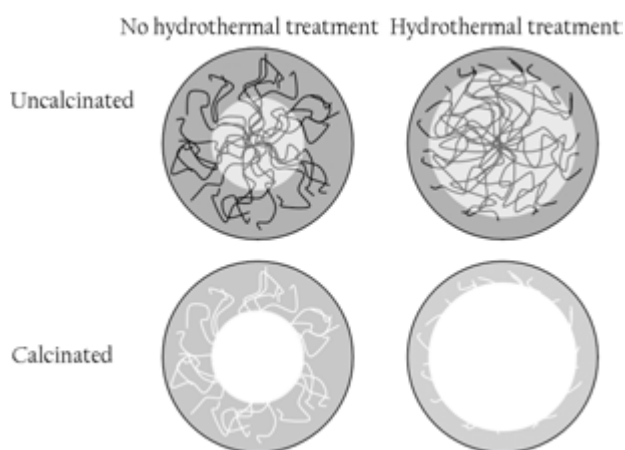


Figure 11. The effect of the hydrothermal treatment.

By increasing the hydrothermal treatment temperature from 35 to 130 °C it is possible to increase the mesopore size with several nanometers, with significant changes noticed above 60 °C [86]. Above this temperature, the microporosity and surface area are decreased and when the treatment is performed at 130 °C no micropores remain and all surface originates from the mesopores. The unit cell parameter is though nearly constant for calcinated samples with hydrothermal treatment temperature exceeding 60 °C, so during the increase of mesopore size the wall thickness decreases and the wall becomes denser and the microporosity is lost [23,86]. Similar effect, but not as pronounced, is obtained by increasing the hydrothermal treatment time.

4.3 Removal of surfactants

The final step of the synthesis is the removal of the surfactants. This is most often done by calcination, but there are alternatives such as chemical removal of the template or decomposition by microwaves, see Figure 12. Regardless of which method used, the aim is always to completely remove the surfactants in a way that is as cheap and time effective as possible.

4.3.1 Calcination

Calcination is the most common way to remove the surfactants from SBA-15. During the calcination, which is performed in air, the material is heated to 550 °C and this temperature is held for 5 h before the material is cooled down to room temperature.

Most of the surfactants decompose between 150-250 °C and at this stage the hexagonal structure retains its size. Above 300 °C water is released and the rest of the polymers are combusted and the hexagonal framework is decreased probably due to condensation in the framework and closing of micropores [89]. During the shrinkage of the hexagonal structure, the mesopore volume is decreased but the micropore volume is almost constant [90]. This indicates that the micropores are still being emptied from surfactant residues simultaneously to the framework shrinkage.

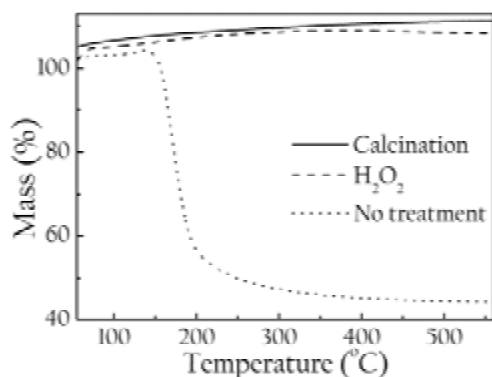


Figure 12. The surfactants can be removed using various techniques, e.g. calcination or oxidation using H₂O₂.

4.3.2 Chemical removal

An alternative route to removal of the surfactants is to oxidize the P123. By using this alternative route there is no shrinkage in the hexagonal structure as it is upon calcination and it is possible to functionalize the material in multiple steps. For this purpose, chemicals such as ethanol, hydrogen peroxide, sulphuric acid or ammonium perchlorate can be used.

Ethanol

Ethanol was used as an alternative to calcination to remove P123 in the first reports of SBA-15 [8,14]. By refluxing the silica in ethanol at 78 °C for 24 h the P123 can be removed. An advantage with this method is that the surfactants are not decomposed but can be recovered and reused for syntheses. Also, there is a larger amount of silanol groups in the silica walls which is preferable when functionalizing the surface. Drawbacks are that there can be residues of P123 in the micropores [91,92] and that large amounts of ethanol are needed during the treatment [93]. The method is suitable for materials where the surfaces have been functionalized during the synthesis process or to functionalize the surface during the ethanol extraction process [94-96].

Hydrogen peroxide

Hydrogen peroxide (H_2O_2) is another oxidation agent that can be used for removal of the surfactants. By treating the SBA-15 with H_2O_2 at 100 °C for 24 h completely removes the polymer template [97]. This method gives a product with slightly larger mesopores, a higher micropore volume and thereby a larger specific surface area. Figure 12 shows that the H_2O_2 treatment is equivalent compared to calcination with respect to surfactant removability. Another difference in the final product is the increased amount of silanol groups in the silica walls when this method is used compared to calcination. Silanol groups can be used as reaction and anchor sites when functionalizing the final product [98]. The H_2O_2 method has been used in Paper I and Paper II.

Sulphuric acid

If instead sulphuric acid (H_2SO_4) is used to remove the surfactants it is possible to control the removal in different parts of the material. H_2SO_4 is selective in the oxidation of the polymer and decomposes only the PPO chains of the surfactant [99,100]. This makes it possible to functionalize the mesopores prior to removing

the PEO chains. The PEO chains are removed by low temperature calcination at 200 °C. Similar to the H₂O₂ treatment, the mesopore size and micropore volume are larger for these samples compared to ordinary calcinated samples. The advantage of this method is that triple functionalized samples can be synthesized with an outer functionalization prior to the first step of the template removal followed by a second and third functionalization in the meso- and micropores respectively.

Ammonium perchlorate

Ammonium perchlorate (AP) mixed with HNO₃ can also be used to selectively remove the surfactants [101]. In this case ethane groups are left on the silica framework. Compared to the H₂O₂ removal of the template, this method is faster since all surfactants are completely removed after 12 h treatment in 80 °C.

4.3.3 Microwave digestion

The fastest method to remove the template from mesoporous silica is to use microwave digestion. When SBA-15 is mixed with HNO₃ and H₂O₂ [91] or alternatively ethanol and hexane [102] and exposed to microwave radiation for 2 min the surfactants are completely removed. These samples also contain higher silanol concentration compared to calcinated samples. Moreover, there is no shrinkage of the framework using this method which yield higher surface area, larger pore size and pore volume compared to calcination [91].

5 TUNING THE PROPERTIES OF SBA-15

SBA-15 can be varied in many ways. Different morphologies can be synthesized, the pore size can be tuned from 5-26 nm and the microporosity, surface area and wall thickness can be varied. It can also form films, either freestanding or on substrates.

5.1 Pore size

As mentioned earlier, the hydrothermal treatment is one way to change the pore size of SBA-15. But with this method, the wall thickness and microporosity are also affected. Other ways to tune the mesopore size are additions of salt, co-surfactants, oils or changing the reaction temperature. All these methods will be discussed in this section.

5.1.1 Swelling agents

A swelling agent is a non-polar reagent that goes into the hydrophobic core of the micelles and expands them, thereby increasing the pore size of the final product. In the first report of SBA-15 1,3,5-trimethylbenzene (TMB) was used as a swelling agent and it was believed that the pore size could be tuned between 5 and 30 nm [14]. But it was later shown that for oil/P123 mass ratios exceeding 0.2 the micelles transform from cylinders to a mesocellular foam (MCF) where spherical pores are attached to each other by smaller windows [58,103]. This is illustrated in Figure 13.

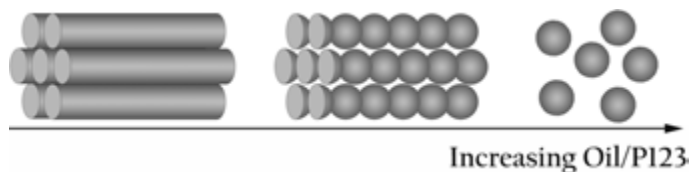


Figure 13. Transition from hexagonal cylinders to MCF by increasing oil content.

When small amounts of oil is added to the synthesis it swells the PPO chains and increase the micelle size. But when the PPO chains are fully saturated the excess oil form pure oil cores in the micelles. The limited amount of P123 must completely cover the oil droplets and therefore the micelle becomes more spherical and the intermediate structure shown in Figure 13 is formed. By further increasing the amount of oil the nodes on the intermediate shape becomes sharper and finally the spheres are separated. The process is driven by the need to decrease the surface-to-volume ratio when the amount of oil to P123 ratio is increased. The maximum pore size for the cylindrical pores when just oil, such as TMB, is added to the synthesis is 12 nm [58]. TMB addition is still the most common way to increase the pore size of SBA-15, e.g. [104-107].

An alternative, but not as efficient, swelling agent is polypropylene oxide (PPO), identical to the hydrophobic block in P123 [108,109]. Additions of this polymer increase the pore size from 4 nm to 5-6 nm depending in the molecular weight of the polymer.

Other hydrocarbons used as swelling agents are alkanes (8-20 carbons) and methyl- or isopropyl-substituted benzene. These can be used as swelling agents following a route similar to the original synthesis and adding the hydrocarbon to the micellar solution prior to the addition of silica precursor [110]. By using the substituted benzene the pore size could be tuned between 7-43 nm, but only MCF were obtained. For alkanes, MCFs were obtained with octane and nonane but with alkanes with 10 or more carbons ordered hexagonal structures were obtained and the pore size could be increased to 10 nm (for decane). The pore size was decreasing with increasing number of carbons in the alkanes.

Shorter alkanes with 6-12 carbons can also be used as swelling agent in a low temperature synthesis in combination with additions of NH_4F . Here many parameters affect the pore size and morphology of the material. This will be discussed in section 5.4.

5.1.2 Co-surfactants

Additions of other surfactants can help tuning the pore size. By adding the cationic surfactant CTAB, the pore size can be decreased from 8.5 to 4.8 nm [111]. The order is though lost but can be regained by additions of NH_4F and KCl. It

was suggested that CTAB causes hydration of the PPO chain in P123 and thereby decreases the hydrophobic volume of the micellar core.

If instead CTAB is added to the synthesis together with TMB, the pore size can be increased up to 12.7 nm [112]. CTAB and ethanol additions are also important for synthesizing spherical SBA-15 particles. This will be discussed in section 5.3.3

5.1.3 Temperature

The pore size is approximately equal to the core radius of the micelles. The core radius is depending on the solution temperature and the CMT. Therefore the pore size can easily be tuned by varying the synthesis temperature. The “normal” synthesis temperature range (30 – 60 °C) the pore size is proportional to the expression

$$R_p \sim (T - T_C)^{0.2} \quad (4)$$

where T is the temperature of the aqueous solution and T_C the CMT [113].

Lowering the temperature decreases the solubility of P123 in water since the hydrophobic PPO chain becomes more hydrated at lower temperatures. This increases CMC and finally only separate surfactants are present in the solution and no micelles are formed. The effect of temperature is seen in the synthesis of SBA-15, for which the pore size can be increased with more than 1 nm when the synthesis temperature is raised with 10 °C [87,114,115].

5.1.4 Silica precursor

Substituting TEOS with sodium metasilicate, a small decrease in pore size can be noticed [73,84]. The reason for this is not discussed, but one explanation can be that there is no ethanol rest product from sodium metasilicate that can expand the hydrophobic core of the micelles. The effect of hydrothermal treatment is though the same regardless of silica source used.

By mixing TEOS with sodium metasilicate in a 4.4 buffer solution the pore size could be tuned from 10 to 16 nm with increasing TEOS/sodium metasilicate molar ratio [74]. Also here there is a transition from ordered hexagonal structures to MCF for larger pores; the maximum d-spacing is 12 nm.

5.1.5 Salt additions

Salts affect the pore size, pore ordering and micropore volume of SBA-15. As mentioned earlier, additions of CTAB as a co-surfactant can be used to tune the pore size but the pore ordering was lost. In this case, additions of NH_4F and KCl made it possible to synthesize highly ordered structures [111]. It is also possible to perform syntheses at lower temperatures when salts are added [61].

Addition of salts also increases the pore size with rising amounts of salt [115-117]. As discussed in section 3.3.3, addition of salts cause dehydration of ethylene oxide units from hydrated PEO from the side of the PPO core. This leads to an increase in the core radius [44,118], and the increase of the hydrophobic part of the micelles induces the formation of micelles and the sphere-to-rod transition which enhances the order of the material and a slight increase in the pore size.

5.2 Wall thickness and microporosity

The thick walls of SBA-15 are one of the things that make this material superior to other mesoporous silicas with the same pore structure. The control of these walls and the microporosity within them are essential for optimizing the material, e.g. walls with low microporosity have higher thermal stability than high porosity walls [119] and adsorption selectivity of hydrocarbons is affected by the microporosity [44,116].

As mentioned earlier, the microporosity is caused by entrapments of PEO chains in the silica walls prior to calcination of the material. Hence, by varying the entrapment of the chains, the microporosity can be tuned.

5.2.1 Hydrothermal treatment and surfactant removal

As described in section 4.2, the wall thickness and microporosity is affected by the hydrothermal treatment. At elevated temperatures, the PEO chains retract into the hydrophobic core of the micelles due to reduced hydration of the chains. This leads to less PEO chains trapped in the silica walls which yield thinner walls with decreased microporosity.

The microporosity and wall thickness is also affected by the surfactant removal technique used, see section 4.3.

5.2.2 Salt additions

Unsurprisingly, addition of salts decreases the wall thickness and micropore volume of SBA-15 [117,120]. The effect of salts is similar to increasing the temperature, as mentioned in section 3.3.3. When sufficient amounts of salts are used in combination with high hydrothermal treatment temperatures, the microporosity is almost completely lost [120].

5.2.3 The SiO₂ to P123 molar ratio

By changing the molar ratio of silica precursor to P123 it is also possible to control the wall thickness, pore size and microporosity. In syntheses performed at lower HCl concentrations (0.1 M) the d-spacing increases with the amount of TEOS. At the same time the pore size and total porosity decreases and at TEOS/P123 molar ratio of 75 the replica of the SBA-15 structure is similar to the ones from MCM-41. The increase of wall thickness is pronounced and is more than doubled when the molar ratio increases from 45 to 75. The lower reaction rate due to the low acidity in the synthesis gives the silica species time to condense on the PEO chains, which if the amount of silica is increased, leads to a decreased PEO-PEO interaction between different micelles [121].

There can though be problems using this technique since plugs of silica can be left inside the mesopores and form constrictions [122-124]. At HCl concentrations common in the synthesis of SBA-15 (-1.4-2 M), only parts of the silica species can react with the PEO chains. The excess silica will penetrate the micellar structure and condense there, forming plugs and constrictions [124]. It should though be noted that the amount of TEOS used in these studies sometimes exceeds the one performed at lower HCl concentration.

5.2.4 Reaction temperature

The microporosity of SBA-15 can be controlled by varying the temperature in the first 10 minutes of the synthesis. Both the hydrophilicity of the PEO chain and the rate of polymerization of TEOS are temperature dependent (see section 3.3.1 and 3.4). When the initial temperature of the synthesis is varied between 28 °C and 55 °C followed by further reaction at 35 °C and hydrothermal treatment at 100 °C, the microporosity in the material decreases with increasing initial temperature [125]. For a fixed hydrothermal treatment time and temperature, variations in microporosity depend on the amount of PEO chains trapped in the

silica network. If the temperature is high when the chains are fixated, they will not penetrate the silica network and the microporosity is reduced. If instead the initial temperature is low, only parts of the silica species will attach to the PEO chains in this stage and after the first 10 minutes of the synthesis the main reaction will occur.

5.3 Morphology

The morphology of SBA-15 can be tuned in many ways, see Figure 14. The most common morphology is the fiber- or rodlike structure where the particles have attached end-to-end. Other structures such as doughnuts, gyroids, rods, platelets and hollow spheres can be synthesized by changing some of the synthesis parameters, e.g. [126,127]. For many applications such as adsorption of biomolecules, short well separated particles are preferable [117].

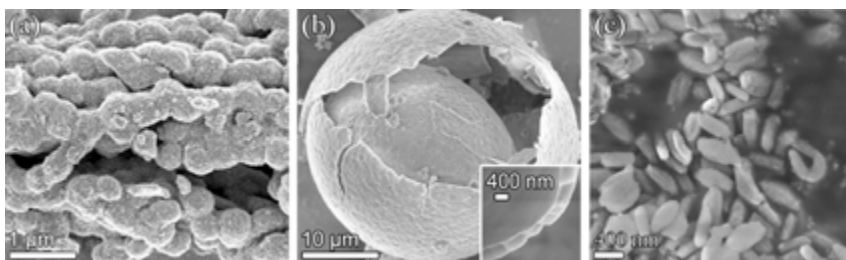


Figure 14. SBA-15 in the form of (a) fiber, (b) hollow sphere and (c) rods.

5.3.1 Rods

A rod is a straight monodispersed particle in which the pores are running through the particle, most often through the long dimension. Most rods are synthesized by decreasing the stirring time from 20 hours to a few minutes and careful control of the synthesis composition.

By decreasing the stirring time from 20 h to 5 min followed by 20 h static condensation of the silica monodispersed silica rods, 1 – 1.5 μm long and ~0.5 μm in diameter, can be synthesized [128]. The morphology was explained by absence of shear flow and a lower rate of precipitation during the static conditions. The same effect has been seen when sodium metasilicate has been used as the silica

precursor. By stirring for times as short as 30 s yields monodispersed rods while stirring through the synthesis results in fiber like morphologies in which the rods act as building blocks [114]. In this study it is also shown that the composition in the synthesis is of great importance for the morphology of the final product. The HCl concentration in both studies was 1.6 mol/l and the amount of silica precursor is also similar. The sizes of the resulting rods are also similar in size and it seems like 1-2 μm monodispersed rods can be synthesized using both TEOS and sodium metasilicate as silica precursor. The pore sizes in these studies have been tuned by varying the hydrothermal treatment time and a range of sizes between 5.5-12.5 nm was obtained. Sodium metasilicate reacts faster than TEOS [129] which can be the reason for the short stirring time required.

Alternatively, addition of inorganic salts such as KCl in combination with stirring for 8 min followed by static condensation for 20 h yield 1-2 μm long straight rods [120]. In this case the HCl to P123 ratio is slightly lower (-316 compared to -348 in the above syntheses). These rods are although not completely separated which can be due to the slightly longer stirring time.

The length of these monodispersed rods can be controlled by varying the amount of HCl and additions of glycerol to the synthesis [130]. A HCl concentration of 2.0 mol/l yields 0.8 μm long and 0.4 μm wide rods while 1.0 mol/l HCl gives 2.5 μm long rods. Further decreasing the HCl concentration increases the length of the rods even more but they start to bend and attach to each other. A similar effect of the HCl concentration with respect to the length of particles forming a rodlike morphology was found when TEOS and BTMSE were used as silica precursors [122].

The decreased length is attributed to the catalytic effect of HCl on the silica precursor [130,131], but it should be noted that a similar effect is not seen when only TEOS is used as the silica precursor. Instead, the additives such as glycerol or BTMSE are necessary for the particle growth.

5.3.2 Platelets

A platelet is a particle in which the base is wider than the height of the particles. These are often hexagonal and have pores going through the short axis of the

particle. This morphology is rare but can be found when P104 is used as surfactant [117,132] or other variations such as salt additions or reduced synthesis temperature are used.

By adding K_2SO_4 to the synthesis and using P104 instead of P123 it is possible to synthesize 300 nm thick hexagonal platelets [117]. Increasing K_2SO_4 concentration yield thinner walls, larger pores, and the thickness to width ratio decreases. Even though it is not mentioned in the paper, it seems like these platelets consist of separate particles attached side by side. The same morphology has been synthesized without K_2SO_4 [132-134].

Additions of $ZrOCl_2$ in varying concentrations also yield 150 – 300 nm thick and 800-1000 wide platelets [135]. It was suggested that the Zr(IV) ions increase condensation rate of TEOS and rods are formed faster compared to syntheses without Zr ions present. Hence, the formation of platelets was preferred to the formation of fibers.

5.3.3 Spherical particles

Spherical particles with ordered pores are commonly hollow, formed around droplets of gas or oils in aqueous solution. Alternatively, solid spherical particles can be synthesized with additions of co-surfactants and co-solvents. This morphology is of interest for applications such as drug delivery systems or storage of gas.

Additions of the co-surfactant CTAB and ethanol yield solid, spherical SBA-15 particles [112,136,137]. Ethanol both decreases the hydrolysis rate of TEOS and reduces the polarity of the aqueous solution which makes it possible to synthesize this morphology [138]. It should though be noted that despite the fact that the PSD is narrow, the pore order is lost in these materials.

The hollow spheres formed around droplets have ordered pores, perpendicular to the particle surface. By controlling the droplet size with e.g. CO_2 [139] or oil concentration [140,141], hollow spheres can be formed. The method of controlling the heptane concentration to form spheres is described in Paper I and II.

5.3.4 Driving forces

SBA-15 particles most commonly attach end to end with each other. But, as previously discussed other particle shapes and morphologies can be synthesized, e.g. particles can be separated, shortened or attached side-by-side.

The particle shape is determined by the relative growth rate of the different planes of the particle [142]. The SBA-15 particles are most often hexagonal with varying lengths and each particle has two (001) and six (100) surfaces, see Figure 15. By varying the synthesis conditions as mentioned previously, the growth rate of the edges can be varied. The height to width ratio is determined by the surface tension of the particle in the relation

$$\frac{h}{w} = \sqrt{3} \frac{\gamma_{001}}{\gamma_{100}}. \quad (5)$$

The ratio can be varied by e.g. changing the synthesis temperature [134].

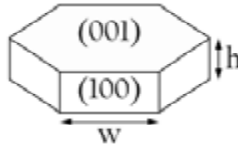


Figure 15. Schematic illustration of a SBA-15 particle with its defined (001) and (100) surfaces.

The mechanism for aggregation between particles to form different morphologies is also related to the surface energies. The basal plane is more hydrophobic than the other planes due to its higher negative surface energy, which is related to the curvature of the micellar caps. Increased temperature or salt additions will lead to a higher energy, yielding longer particles. To reduce the energy, there is an end-to-end attachment between particles [143].

The end-to-end attachment is also favoured by the active hydroxyl groups on the (001) surface. During the silica precursor polymerization, the number of hydroxyl groups responsible for attaching particles to each other is diminished. This passivation is more severe for the mantle surface since the hydroxyl groups at the ends are relatively shielded from the acid by the micelles. A higher acid

concentration gives a stronger passivation and thereby particles can be separated and form rods [130].

5.4 Alkanes and NH_4F in a low temperature synthesis

By combining the effects of low temperature, salt additions and swelling agents, SBA-15 with pores larger than 12 nm can be synthesized in varying morphologies [21,22,62,140,141]. This synthesis route, or variations of it, is used in Papers I – III.

5.4.1 Pore sizes

The large pore size is a result of the combination of low temperature, oil additions and salt. The amount of alkanes in these studies greatly exceeds the amount of TMB that induces the phase transformation from ordered hexagonal structures to MCFs. This is due to the effect of low temperature and additions of NH_4F .

The alkanes can be varied from pentane to hexadecane and the pore size depends on the alkane used. The large pore size is dependant on the alkane used and varies from 12 nm (dodecane) to 15.7 nm (hexane) [63]. By varying the hydrothermal treatment time and temperature it has been possible to tune the pore size between 9-18 nm when hexane was used as swelling agent [88].

Recently, low temperature studies, similar to the alkane studies, was performed in which the alkanes were exchanged for 1,3,5-triisopropylbenzene (TIPB) [19,20]. This resulted in 26 nm large pores which is the largest pore size for SBA-15 until now.

5.4.2 Morphologies

The pore length, and thereby particle size, depends on the alkane used. Shortest pores with ~150 nm are obtained with nonane in comparison with 800–1 000 nm for dodecane or without alkanes [63]. This variation is due to the different solubility of the alkanes in the micelles. At a fixed temperature, larger amounts of short alkanes can be dissolved in the core of the micelles [144]. The quantity of alkane in the core affects the length of the rods in the sphere-to-rod transitions. Hence, a larger amount of alkane (shorter alkane chain) yields shorter pores.

Even though the particle length varies, the fiberlike structure is still the most common morphology [63].

By increasing the amount of decane in the synthesis, the particles forming the fiber morphology can be separated. Further additions of decane yield cuboid particles [63]. In the cuboids, the pores are not running through the long axis of the particle, but through the short axis. This is due to the high amount of oil in the solution. In all alkane syntheses, excess oil than needed to swell the micelles is used. The extra oil is forming discrete spaces between the cuboids and hinder the end to end attachment between the particles [21]. The similar effect is seen in Paper I and II, where excess of heptane forms droplets in the aqueous solution and acts as a structure directing agent during the formation of SBA-15 sheets.

Increasing the amount of TEOS at a fixed concentration of decane will change the morphology from fiberlike to platelets and further to freestanding films [63]. In the platelets, the pores are accessible from the basal surface of the particle whereas in the films, the pores are running along the film surface. If instead the concentration of TEOS is decreased and octane is used as swelling agent, small separate particles, 50–80 nm wide and 100–200 nm long can be synthesized [22]. The mechanisms for these morphology transitions are still unclear.

5.5 Films

Mesoporous films are of great interest when it comes to applications such as catalysts, solar cells and batteries. One of the biggest challenges regarding SBA-15 film synthesis is the pore orientation. The cylindrical pores of SBA-15 are most often aligned parallel to the film surface [145]. There are several ways to synthesize these films, e.g. Evaporation-Induced Self-Assembly (EISA) by dip- or spin-coating, self-formed films in the solvent/air or solvent/oil interfaces [146].

5.5.1 Evaporation-Induced Self-Assembly

Evaporation-Induced Self-Assembly (EISA) is the most common method for synthesizing mesoporous silica films, and it is used for e.g. spin or dip coating. In EISA, the start solvent consists of a silica precursor and surfactants dissolved in a water/ethanol solution. The surfactant concentration is here below CMC. By varying the initial composition of the surfactant containing solution, it is

possible to vary the structure of the final film. A substrate is alternatively dipped and withdrawn from the solution or the solution is spin coated onto the substrate, commonly silicon wafers or glass substrates. After deposition of the solution onto the substrate, the ethanol evaporates and the concentration of water and surfactants increase. Hence, the surfactant concentration increases above CMC and micelles start to form on the substrate [147-149]. The process is illustrated in Figure 16.

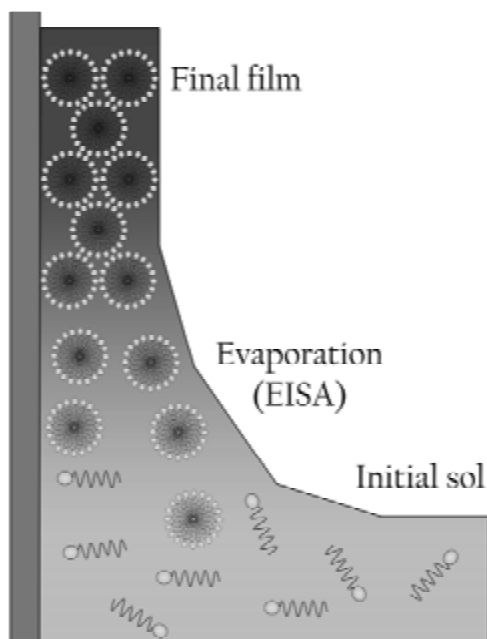


Figure 16. The formation of ordered structures in mesoporous films using EISA.

With EISA and standard substrates, the pores are always oriented with the long axis parallel to the substrate. The thickness of the films can be controlled by varying the deposition rate of the films and the amount of solvent in the solution [150]. For thin films (thickness < 200 nm) it is possible to control the horizontal orientation of the cylinders by controlling the flow direction of the solution [151]. Alternatively, the pores can be oriented by laser induced patterns on the substrate [152]. But it is still not possible to create a film with cylindrical pores perpendicular to the substrate using this method.

5.5.2 Substrate manipulation

One way to control the orientation of the cylindrical pores is to manipulate the substrate surface.

By using alumina substrates with conical holes the orientation of the mesopores can be changed from parallel to perpendicular to the substrate by changing the depth and width of the conical holes [153]. Holes with small aspect ratio are filled with sponge-like mesostructures which yields films with perpendicular and tilted cylinders. These cylinders start to grow from the mesostructures in the holes. When the aspect ratio is increased, the conical holes are filled with cylindrical mesopores in a doughnut like stacking which acts as the start for mesoporous films with pores running parallel to the substrate.

It has been shown that surface modifications can tune the pore orientation of mesoporous films [154]. By using octadecyltrichlorosilane (OTD) to make the surface of silicon wafers more hydrophobic it has been possible to synthesize thin mesoporous films in which the pores are like craters -40 nm wide but only -1 nm deep. The width of these craters corresponds well with the length of the extended P123 molecule.

In Paper III we have used silicon wafers treated to be hydrophilic or hydrophobic. This hopefully results in good control of the pore orientation in the synthesized mesoporous film.

5.5.3 Freestanding films at interfaces

When an SBA-15 film is formed at an oil/water or water/air interface it is possible to align the pores perpendicular to the film surface.

Exchanging HCl for H_3PO_4 gives the possibility to form films in the air/water interface under static conditions. In the solution, cakelike structures consisting of agglomerated particles are formed. If instead stirring is used, the common fiberlike structure is formed [155,156].

By creating a bilayer of C_{16}MTAB and SDS micrometer large platelets < 200 nm thick with pores perpendicular to the surface has been synthesized. By drying some of the synthesis solution on a silicon wafer, a mesoporous film with

preferable pore orientation was synthesized [157]. However, by random drying of solution onto the substrate, there is very low control of how the particles attach to the substrate and overlapping of particles is common.

6 ANALYSIS TECHNIQUES

There is not one universal analysis technique that provides all information necessary to characterize a porous material. The surface area, pore size, pore volume, and, to some extent, pore shape of the materials are measured using physisorption with N_2 gas but this technique does not reveal the pore order. This information is instead given by X-ray diffraction (XRD) and transmission electron microscopy (TEM). The particle morphology is imaged using scanning electron microscopy (SEM) and in some cases even the mesopores can be resolved and seen here. The functional groups attached to the material walls have been studied with Fourier transformed infrared spectroscopy (FT-IR).

6.1 Physisorption

Gas sorption is a technique used for characterizing porous materials. With this method a materials specific surface area, pore volume and pore size distribution can be determined.

6.1.1 Physisorption isotherms

The physisorption data is presented in sorption isotherms with the amount of gas adsorbed on the solid plotted versus the relative pressure. The isotherms can be grouped into six types [1] which are shown in Figure 17.

Type I isotherms: This type is characteristic for microporous materials. In micropores there is an increased adsorbent-adsorbate interaction. The nearly horizontal plateau is reached at low relative pressures which indicate a small external surface area.

Type II isotherms: These isotherms are typical for non-porous, microporous and macroporous materials. Here there is a monolayer-multilayer adsorption on an open and stable surface. The knee-point at B indicates where the monolayer adsorption is complete and multilayer adsorption begins. B indicates the material's monolayer capacity as it is measured how much adsorbate is required to cover the unit mass of solid surface with a monolayer of adsorbate molecules.

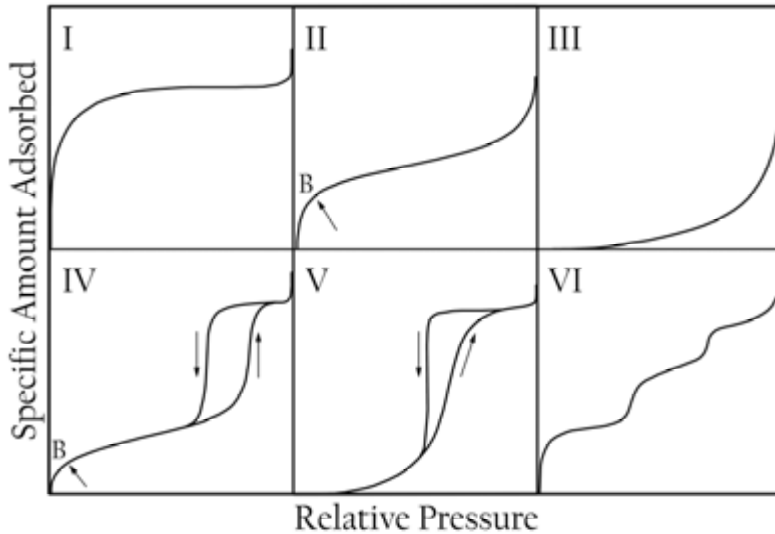


Figure 17. The six main types of adsorption isotherms according to IUPAC classification [1].

Type III isotherms: These isotherms are very uncommon and are characteristic for materials with very weak adsorbate-adsorbent interactions.

Type IV isotherms: This type of isotherm is typical for porous materials. At the beginning the isotherm is similar to the type II isotherms. The knee-point at B indicates here, as well as for type II isotherms, the monolayer capacity of the material. At higher pressures, there is a hysteresis loop, for different types of hysteresis loops see Figure 18, which is characteristic for type IV isotherms.

Type V isotherms: The type V isotherms are characteristic for porous materials with weak adsorbate-adsorbent interactions. Initially they are similar to the type III isotherms but at higher pressures there is a hysteresis loop.

Type VI isotherms: These isotherms are due to layer-by-layer adsorption on a highly uniform surface. The steps are formed by separate layers adsorbing onto each other.

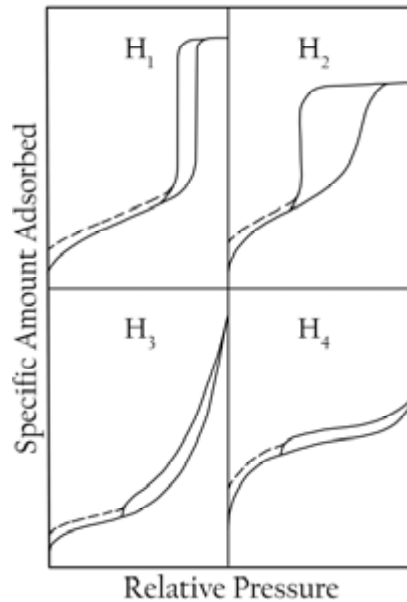


Figure 18. The four main types of hysteresis loops according to IUPAC classification [1].

The four types of hysteresis loops, seen in Figure 18, indicate how the pores are shaped and if there are any inclusions or plugs in them.

H1: This type of hysteresis loop has steep parallel adsorption and desorption isotherms. At these steps all pores are filled (adsorption) and emptied (desorption). It is typical for mesoporous materials with uniform pores.

H2: The *H2* hysteresis loop has a smoother adsorption step and a sharp desorption step. It is typical for materials with nonuniform pore shapes and/or sizes, e.g. silica gel or other metal oxides.

H3: This type of hysteresis loop is associated with slit-shaped pores. These often rise from agglomerates of plate-like particles.

H4: The *H4* hysteresis loop is similar to *H3* but has a more horizontal plateau which indicates microporosity in the material.

6.1.2 Specific surface area determination, the BET method

The most frequently used procedure to determine the surface area of a porous material is the Brunauer-Emmet-Teller (BET) method [158]. The method has evolved from the Langmuir theory [159] with multilayer corrections. It is assumed that

1. the adsorbent surface is uniform and all adsorption sites are equivalent
2. adsorbed molecules do not interact
3. all adsorption occurs through the same mechanism
4. at the maximum adsorption, only a monolayer is formed: molecules of adsorbate do not deposit on other adsorbed molecules of adsorbate, only the free surface of the adsorbent.

To calculate the BET surface area the monolayer capacity, n_m , of the material is determined from the BET-plot. This is the best linear fit of the adsorption isotherm that includes the B point, see Figure 17, and is derived by the linear BET equation

$$\frac{P/P_0}{n(1-P/P_0)} = \frac{1}{n_m C} + \frac{C-1}{n_m C} \cdot \frac{P}{P_0} \quad (6)$$

where P/P_0 is the relative pressure, n the amount adsorbed and n_m the maximum amount adsorbed i.e. the monolayer capacity and C a system dependent constant. A sharp point B is indicative of a high value of C and thereby of a high adsorbent-adsorbate interaction.

The BET specific surface area is then calculated by

$$a_s = \frac{A_s}{m} = \frac{n_m N_A \sigma}{m} \quad (7)$$

where a_s is the specific surface area, A_s the total surface area, m the mass of the sample, N_A Avogadro's number and σ the molecular cross-sectional area occupied by the adsorbate molecule in the complete monolayer [1,160].

6.1.3 Micropore volume and external surface area

Each adsorbate-adsorbent system yields a unique isotherm due to variations in the interaction between the species. Therefore each system needs a standard isotherm to estimate the micropore volume, internal and external surface area. The standard isotherm can also be used as a reference for adsorbed layer thickness. This isotherm is measured for a nonporous sample of the same material as the specimen analyzed. For silica, standard nitrogen adsorption data for LiChrospher Si-4000 silica is available for the P/P_0 $5.55 \cdot 10^{-7}$ -0.988 [161] as a standard isotherm.

In this work, the micropore volume was estimated by using a t -plot [162], see Figure 19. The thickness of the adsorbed layer is determined by

$$t = t_m \frac{n}{n_m} \quad (8)$$

where t_m is the thickness of a monolayer, for nitrogen $t_m = 3.54 \text{ \AA}$. In order to relate the layer thickness to the relative pressure, several methods can be used, e.g. the Halsey [163], Harkins and Jura [164] or Broekhoff-de Boer methods, or the reference isotherm.

When using the KJS method, the Harkins-Jura equation

$$t \left(\frac{P}{P_0} \right) = 0.1 \left[\frac{60.65}{0.03071 - \log \frac{P}{P_0}} \right]^{0.3968} \quad (9)$$

is used to determine the thickness.

To determine the micropore volume and external surface area, the volume adsorbed is plotted against the t . The micropore volume is found as the intercept of the extrapolated first linear region of the t -plot and the y -axis and the external surface area (the surface area from meso- and macropores and the true external surface) is determined as the slope of the second linear region, see Figure 19.

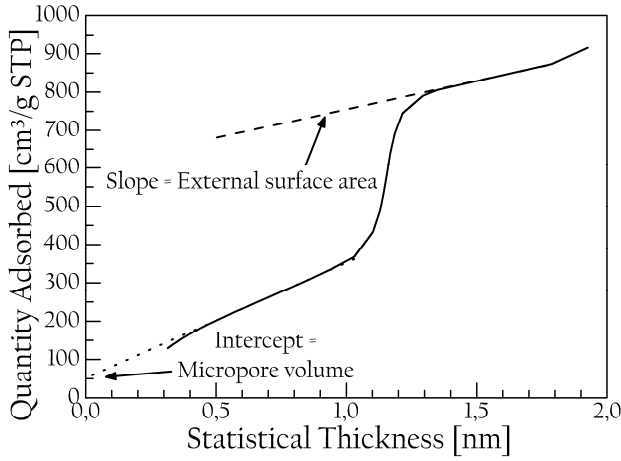


Figure 19. t-plot for SBA-15.

6.1.4 Mesopore size analysis

There are several methods, such as the BJH [165], BdB [166-169] or KJS [170,171] methods, alternatively NLDFT [172-174], used to determine the pore size distribution (PSD) from nitrogen sorption isotherms. Different methods are suitable for different pore shapes and sizes. In this work, only the KJS-method has been used.

The main principles for calculating pore sizes are based on the concept of capillary condensation and the Kelvin equation

$$\ln \frac{P}{P_0} = -\frac{2\gamma V_L}{RT} \left(\frac{\cos \theta}{r_K} \right) \quad (10)$$

where γ is the surface tension of the adsorptive liquid, V_L the molar volume of the liquid, θ the contact angle between the solid and the condensed phase and r_K the mean radius of the liquid meniscus. When a critical pressure is reached, the adsorptive will condensate in the pores. Hence, the pore radius will determine if condensation can occur at a given pressure as illustrated in Figure 20. This is seen as the hysteresis loop from the physisorption data.

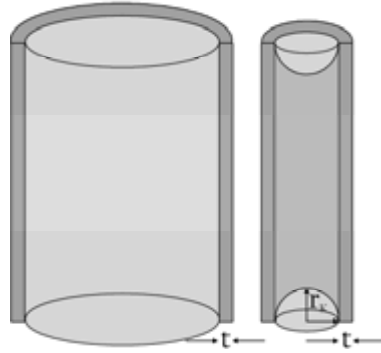


Figure 20. Capillary condensation at a given pressure is determined by the pore radius. The pore size is given by $2 \cdot (r_K + t)$.

The BJH method

Most calculation methods are based on the Barrett-Joyner-Halenda (BJH) method. Here, it is assumed that all pores have a cylindrical shape, that the simple Kelvin equation (eqn. (10)) is applicable, the meniscus is hemispherical with $\theta=0$ and that the correction for multilayers is valid.

For capillary condensation in cylindrical pores, the Kelvin radius as a function of relative pressure can be written as

$$r_K \left(\frac{P}{P_0} \right) = - \frac{2\gamma V_L}{RT \ln \frac{P}{P_0}} \quad (11)$$

The pore size, r_p , is then obtained by adding adsorbed layer thickness, t , to r_K [160], so the pore width is

$$r_p = 2 \cdot (r_K + t) \quad (12)$$

For each step in the isotherm, the difference in amount of adsorptive represents the core volume filled or emptied in that step. The thickness of the adsorbed layer remaining on the pore walls is calculated with some method, this will be discussed in following paragraph. Using eqns.

(11) and (12) the pore size can now be calculated.

To decide the amount of pores with this size, the shape of the pores is assumed to be homogenous for all pores, e.g. cylindrical. Using the difference in core volume and the volume of a cylinder with the radius r_p , the total length of pores with this radius can be calculated. From this, the area of these pores can be calculated. By performing these calculations for all steps in the isotherms, the total PSD can be obtained.

The KJS method

This method was developed in the late 90's to improve the PSD from the BJH method. It is based on the BJH method and uses the Kelvin equation and Harkins-Jura thickness equation. Furthermore, the sum in eqn. (12) underestimates the pore size with -0.3 nm. Hence, the final expression for the pore size [nm] is according to the KJS-method

$$r_p \left(\frac{P}{P_0} \right) = \frac{2\mathcal{W}_L}{RT \ln \frac{P}{P_0}} + 0.1 \left[\frac{60.65}{0.03071 - \log \frac{P}{P_0}} \right]^{0.3968} + 0.3. \quad (13)$$

The method was first developed and calibrated for MCM-41 with maximum 6.5 nm pores. This led to an overestimation of 1-2 nm in pore size when measuring on SBA-15 [175] and therefore a correction for larger pore sizes was made to the method [171]. The pore size is now calculated as

$$r_p \left(\frac{P}{P_0} \right) = -\frac{1.15}{\log \left(0.875 \frac{P}{P_0} \right)} + 0.2 \left[\frac{60.65}{0.03 - \log \frac{P}{P_0}} \right]^{0.397} + 0.27. \quad (14)$$

6.1.5 Porosity

The porosity of a material is determined by the total pore volume divided with the volume of the material. The total pore volume, v_p , is taken as the liquid volume adsorbed at a given pressure e.g. $P/P_0 = 0.99$. Since the amount adsorbed by the material when $P/P_0 \rightarrow 1$ depends on the magnitude of the external area and the upper limit of the pore size distribution this method is not always satisfying. [160]. In the case of a type IV isotherm there is often a horizontal plateau after

the filling of the mesopores. It is generally assumed that the amount adsorbed at this plateau is a measure of the adsorption capacity.

6.2 X-Ray Diffraction

X-ray diffraction (XRD) is a technique used to study periodically ordered structures at atomic scales. The wavelengths of X-rays are in the same order of magnitude as the distance between lattice planes in crystalline materials. When the X-rays enter the material they will be scattered by the electron clouds around the atoms. The periodicity of the lattice planes gives rise to constructive interference of the X-rays, see Figure 21, and the intensity of the scattered X-rays is plotted against the angle 2θ . From the plotted peaks the lattice distance can be calculated using Bragg's law

$$n\lambda = 2d_{hkl} \sin \theta \quad (15)$$

where n is the order of diffraction, λ the wavelength, d_{hkl} the distance between lattice planes and θ the angle of the incoming light.

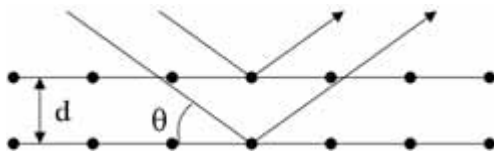


Figure 21. Schematic illustration of diffraction according to Bragg's law.

SBA-15 has a hexagonally ordered pore structure. As illustrated in Figure 22, the unit cell size, a , can be calculated from the first Bragg peak position

$$a = \frac{2}{\sqrt{3}} d_{100}. \quad (16)$$

For crystalline materials the lattice planes are often in the order of a couple of Å which gives a scattering angle of $\sim 20^\circ$ if $\text{CuK}\alpha$ radiation ($\lambda = 1.54 \text{ \AA}$) is used and scans between $20\text{-}80^\circ$ are common for characterization of the atomic structure of the material. For amorphous materials, such as mesoporous silica, there are no periodic atomic planes but the technique is still useful for characterization of the ordered pore structure.

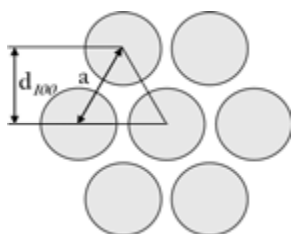


Figure 22. Schematic illustration of a hexagonal structure with the d_{100} spacing and unit cell parameter a .

Mesoporous materials with periodically ordered pores give reflections for low angles, $2\theta < 3^\circ$, see Figure 23. These low angles makes detection by reflection difficult since some of the X-ray beam can go straight into the detector and cause high background radiation which makes it difficult to see and identify the peaks. Therefore a transmission detector is preferable when measuring on mesoporous materials.

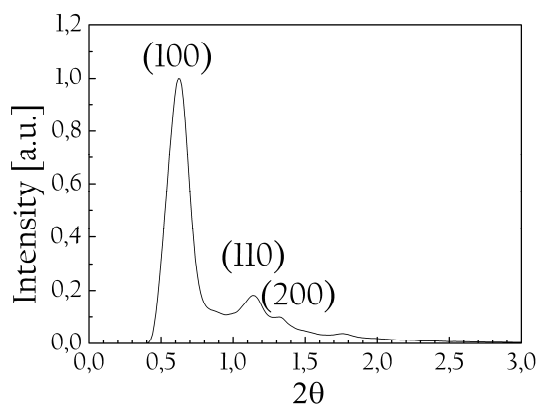


Figure 23. XRD pattern for SBA-15.

6.3 Electron Microscopy

For studies of the pore structure and particle morphology of the materials electron microscopy is used to visualize the structures. Optical microscopes do not have sufficient resolution to picture the particle morphology. Furthermore,

physisorption and XRD is not enough to characterize the pore structure since there can be mixtures of pore orderings or regions with unordered pores.

The smallest distance between two objects that can be resolved is described by the Rayleigh criterion

$$d = 0.62 \frac{\lambda}{n \sin \theta} \quad (17)$$

where d is the resolution, λ the wavelength, n the refractive index of the medium and θ the angle of the collected light. Using an acceleration voltage of 200 keV gives the electrons a wavelength of -1 pm which gives a much higher resolution compared to optical microscopes where the wavelength is -100 nm. Both scanning and transmission electron microscopes can be used for both structural and elemental analysis but only the techniques used in this work will be mentioned here.

6.3.1 Scanning Electron Microscopy

Scanning electron microscope (SEM) is used to study the topography of materials, see Figure 24 (a), and has a resolution of -2 nm. An electron probe is scanning over the surface of the material and these electrons interact with the material. Secondary electrons are emitted from the surface of the specimen and recorded. The height differences in the sample give contrast in the image. In this work, SEM has been used to study morphology of the particles and the pore direction in the mesoporous films.

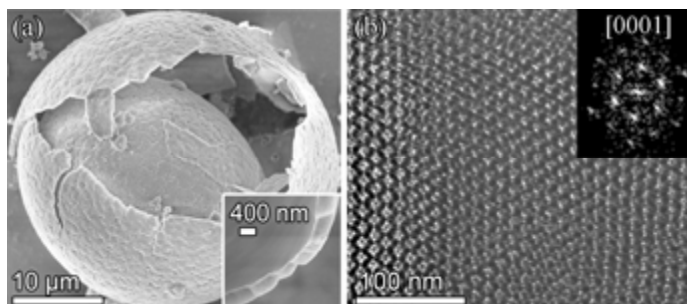


Figure 24. Micrographs and Fourier transform of SBA-15 sheets imaged using (a) SEM and (b) TEM.

6.3.2 Transmission Electron Microscopy

With transmission electron microscopy (TEM) it is possible to resolve features in the range of 1 Å. In a TEM a beam of electrons is transmitted through a thin sample and the electrons are scattered in the specimen. The transmitted electrons are focused on a fluorescent screen or CCD camera by electromagnetic coils and the image is formed. The image contrast originates from mass-thickness differences where thicker regions of the specimen (in this case the silica walls) absorb or scatter more of the electrons compared to thinner regions. Furthermore, it is possible to increase the contrast by blocking out some of the diffracted beams which will result in an image where areas that strongly diffract the electrons (here again, the silica walls) will appear darker in the micrograph.

Fast fourier transforms (FFT) of the TEM micrographs gives the diffraction pattern of the specimen. This is similar to the information given by XRD but it is calculated from the micrograph and not measured from the whole sample. It can be used to study, e.g. grain orientations in poly-crystalline materials or pore structures in the mesoporous silica. In this work TEM and FFT has been used to study the pore structure of the materials, an example is shown in Figure 24 (b).

6.4 Thermogravimetric Analysis

Thermogravimetric analysis (TGA) is used to study mass changes in a material due to changes in temperature. It is used to study e.g. oxidation of materials or, as in this case, decomposition of polymers.

The sample is placed on a high-precision balance and subsequently heated following a given temperature program. Varying atmospheres such as air, argon or helium can be used depending on the purpose of the measurement. During the heating, the sample weight is plotted against temperature.

An example of TGA results is shown in Figure 12 where different techniques for removal of surfactants in SBA-15 are studied. In this study TGA and FT-IR were used to study if the surfactants were completely removed by H₂O₂ and the results were compared to results from calcinated and uncalcinated samples. The heating program was similar to the calcination program with a temperature ramp of 10 °C/min up to 550 °C and then held there for 1 h.

6.5 Fourier Transformed Infrared Spectroscopy

Fourier transformed infrared spectroscopy (FT-IR) is used to study functional groups on the surface of materials using the discrete energy levels for vibrations of atoms in these groups. In this work FT-IR has been used to compare different techniques to remove P123.

When light with a specific energy is transmitted through the sample it can be absorbed by groups of atoms in the material. This occurs when the frequency of the incoming light corresponds to the frequency of vibrations in bonds between atoms. The vibration energy depends on the masses and chemical environment of the atoms, the type of vibration.

By scanning over a range of wavelengths (in this case $400\text{-}4\,000\text{ cm}^{-1}$) and recording the amount of transmitted light for each wavelength it is possible to determine which functional groups that are present on the surface of the material.

7 SUMMARY OF RESULTS

7.1 Paper I

In this letter the synthesis of SBA-15 with 18 nm large pores in a sheet morphology is reported. When heptane is added to a low temperature synthesis of SBA-15 the oil goes into the hydrophobic core of the micelles and expands them. The oil also acts as a structure directing agent for the SBA-15 crystallites which attach to each other mantle surface to mantle surface, forming the sheet morphology.

7.2 Paper II

In this paper it is reported how heptane additions in a low temperature synthesis of SBA-15 affect the pore size and morphology of the material. The pore size was further increased by removing the surfactants using H_2O_2 instead of calcination. It was shown that heptane is acting as a pore swelling agent, resulting in 13-18 nm large pores ordered in a hexagonal structure. Also, the material consists of crystallites with ordered pores running through them. Heptane is acting as a structure directing agent for the crystallites, as can be seen in Figure 25, which results in two morphologies: fibers and sheets.

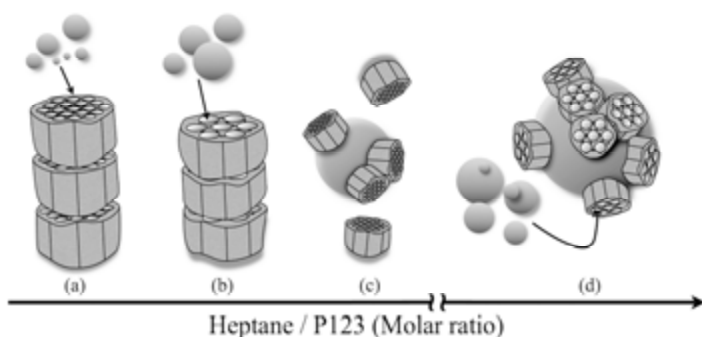


Figure 25. Schematic illustration of the role of heptane during the formation of different morphologies of SBA-15 [141].

For both morphologies the pore size increases with increasing heptane to P123 molar ratio. At the morphological transition there is a drop in pore size due to that the crystallites rearrange around and stabilize heptane droplets in addition to swelling the micelles. Furthermore, we showed that H_2O_2 can be used to completely remove P123 and thereby avoid shrinkage of the framework upon calcination. This allows for an even larger pore size to be obtained.

It was also shown that the pore order can be controlled by tuning the water to P123 molar ratio. Small changes of the water amount in the range of 33.5 – 37.5 ml drastically change the pore structure from disorder to hexagonally order and back to disorder.

7.3 Paper III

This paper shows that it is possible to synthesize large pore, well dispersed SBA-15 rods in a rapid synthesis. Also in this paper, a low temperature synthesis and additions of heptane and NH_4F were used to increase the pore size.

The separation of particles is performed by decreasing the stirring from the normal 20 h to 4 min. This stirring is followed by keeping the synthesis solution at 20 °C under static conditions prior to the hydrothermal treatment. The static time was varied between 0 and 180 min, and it was shown that only 60 min is needed to gain a well ordered material with similar pore size and surface area as the 180 min sample. Hence, this method makes it possible to synthesize well dispersed, ordered rods in less than 1 h compared to the previous 20 h.

Furthermore, the length and width of the particles can be controlled by variations in the HCl concentration. This is due to the effect of HCl on the hydrolysis rate of TEOS. A higher HCl concentration increases the hydrolysis rate which leads to an earlier passivation of the hydroxyl groups on the mantle surface of the particles. Due to this early passivation, less micelles can attach to each other and the final particle shape is thinner. Simultaneously, the rapid hydrolysis rate increases the formation rate of cylindrical micelles. Hence, at higher HCl concentrations, the micelles are more elongated, narrow and more homogenous in length compared to those synthesized with lower HCl concentrations.

Finally, the pore size was controlled by changes in the hydrothermal treatment time and/or temperature. As previous reports have shown, the pore size increases with increasing hydrothermal treatment time and/or temperature. Hence, for a given HCl concentration, the pore size could be varied between 11 and 17 nm.

8 CONCLUSIONS

Mesoporous silica with cylindrical, hexagonally ordered pores can be synthesized using non-ionic triblock copolymers in a sol-gel synthesis. The pore size and morphology of this material can be controlled by variations in the synthesis conditions. By using a reaction temperature of 20 °C and additions of heptane and NH_4F , it is possible to increase the pore size from the normal 6-12 nm to 18 nm. The material is formed by crystallites, which can be attached end to end to form fibers, side by side to form sheets, and as separated rods.

The pore size can mainly be controlled by variations in heptane concentration and hydrothermal treatment time and/or temperature. Increasing one or more of these parameters yield a larger pore size. A smaller variation in pore size is also observed by increasing the HCl concentration.

Heptane acts as both swelling agent for the micelles and structure directing agent for the crystallites. When the heptane droplets in the synthesis solution have reached a critical size, the crystallites turn their hydrophobic ends towards them and the sheet morphology is formed. For lower amounts of heptane, the crystallites instead attach end to end, and a fiber-like morphology is formed.

Separate rods are formed when the stirring time is decreased from 4 h to less than 5 min, in combination with an increased HCl concentration. The increased HCl concentration is crucial for the formation of ordered structures since it affects the hydrolysis rate of the silica precursor. The time for static conditions prior to the hydrothermal treatment for the rods can be decreased to less than 1 h, and the material shows an ordered pore structure after a static time of 5 min.

Additionally, it was shown that the surfactants can be completely removed by H_2O_2 as an alternative to calcination and that the water concentration is crucial when synthesizing materials with an ordered pore structure at high heptane concentrations.

9 REFERENCES

- [1] K.S.W. Sing, D.H. Everett, R.A.W. Haul, L. Moscou, R.A. Pierotti, J. Rouquérol, T. Siemieniewska, *Pure & Appl. Chem.* 57 (1985) 603-619.
- [2] C.T. Kresge, M.E. Leonowicz, W.J. Roth, J.C. Vartuli, J.S. Beck, *Nature*. 359 (1992) 710-712.
- [3] P. Yang, D. Zhao, D.I. Margolese, B.F. Chmelka, G.D. Stucky, *Nature*. 396 (1998) 152-155.
- [4] F. Jiao, P.G. Bruce, *Angewandte Chemie International Edition*. 43 (2004) 5958-5961.
- [5] S. Jun, S.H. Joo, R. Ryoo, M. Kruk, M. Jaroniec, Z. Liu, T. Ohsuna, O. Terasaki, *J. Am. Chem. Soc.* 122 (2000) 10712-10713.
- [6] R. Ryoo, S.H. Joo, M. Kruk, M. Jaroniec, *Adv. Mater.* 13 (2001) 677-681.
- [7] J.S. Beck, J.C. Vartuli, W.J. Roth, M.E. Leonowicz, C.T. Kresge, K.D. Schmitt, C.T. Chu, D.H. Olson, E.W. Sheppard, C.T. McCullen, J.B. Higgins, J.L. Schlenker, *J. Am. Chem. Soc.* 114 (1992) 10834-10843.
- [8] D. Zhao, Q. Huo, J. Feng, B.F. Chmelka, G.D. Stucky, *J. Am. Chem. Soc.* 120 (1998) 6024-6036.
- [9] I. Kartini, P. Meredith, J.C. Diniz da Costa, J.D. Riches, G.Q.M. Lu, *Curr. Appl. Phys.* 4 (2004) 160-162.
- [10] S.H. Joo, S.J. Choi, I. Oh, J. Kwak, Z. Liu, O. Terasaki, R. Ryoo, *Nature*. 412 (2001) 169-172.
- [11] M. Kruk, M. Jaroniec, T. Kim, R. Ryoo, *Chem. Mater.* 15 (2003) 2815-2823.
- [12] V. Chiola, J.E. Ritsko, C.D. Vanderpool, 3556725 (1971).
- [13] F. Di Renzo, H. Cambon, R. Dutartre, *Microporous Materials*. 10 (1997) 283-286.
- [14] D. Zhao, J. Feng, Q. Huo, N. Melosh, G.H. Fredrickson, B.F. Chmelka, G.D. Stucky, *Science*. 279 (1998) 548-552.
- [15] S.A. Bagshaw, E. Prouzet, T.J. Pinnavaia, *Science*. 269 (1995) 1242-1244.

- [16] R. Ryoo, J.M. Kim, C.H. Ko, C.H. Shin, *J. Phys. Chem.* 100 (1996) 17718-17721.
- [17] C. Yu, Y. Yu, D. Zhao, *Chemical Communications.* (2000) 575-576.
- [18] S. Che, A.E. Garcia-Bennett, T. Yokoi, K. Sakamoto, H. Kunieda, O. Terasaki, T. Tatsumi, *Nature Materials.* 2 (2003) 801-805.
- [19] L. Cao, T. Man, M. Kruk, *Chem. Mater.* 21 (2009) 1144-1153.
- [20] L. Cao, M. Kruk, *Colloids Surf. Physicochem. Eng. Aspects.* 357 (2010) 91-96.
- [21] H. Zhang, J. Sun, D. Ma, X. Bao, A. Klein-Hoffman, G. Weinberg, D. Su, R. Schlogl, *J. Am. Chem. Soc.* 126 (2004) 7440-7441.
- [22] J. Sun, H. Zhang, R. Tian, M. Ding, X. Bao, D.S. Su, H. Zou, *Chem. Comm.* (2006) 1322-1324.
- [23] M. Impérator-Clerc, P. Davidson, A. Davidson, *J. Am. Chem. Soc.* 122 (2000) 11925-11933.
- [24] R. Ryoo, C.H. Ko, M. Kruk, V. Antochshuk, M. Jaroniec, *J. Phys. Chem. B.* 104 (2000) 11465-11471.
- [25] M. Kruk, M. Jaroniec, C.H. Ko, R. Ryoo, *Chem. Mater.* 12 (2000) 1961-1968.
- [26] S. Ruthstein, V. Frydman, S. Kababya, M. Landau, D. Goldfarb, *J. Phys. Chem. B.* 107 (2003) 1739-1748.
- [27] C. Göltner-Spickermann, *Curr. Opin. Colloid Interface Sci.* 7 (2002) 173-178.
- [28] L. Vradman, L. Titelman, M. Herskowitz, *Microporous Mesoporous Mater.* 93 (2006) 313-317.
- [29] A.-. Lu, W.-. Li, W. Schmidt, W. Kiefer, F. Schüth, *Carbon.* 42 (2004) 2939-2948.
- [30] A.B. Fuertes, *Microporous and Mesoporous Materials.* 67 (2004) 273-281.
- [31] M. Tiemann, *Chemistry of Materials.* 20 (2008) 961-971.
- [32] M. Armandi, B. Bonelli, E.I. Karaindrou, C.O. Areán, E. Garrone, *Catalysis Today.* 138 (2008) 244-248.
- [33] H. Zhou, S. Zhu, I. Honma, K. Seki, *Chemical Physics Letters.* 396 (2004) 252-255.

- [34] G. Satishkumar, L. Titelman, M.V. Landau, *Journal of Solid State Chemistry*. 182 (2009) 2822-2828.
- [35] W. Yue, W. Zhou, *Progress in Natural Science*. 18 (2008) 1329-1338.
- [36] A. Taguchi, F. Schüth, *Microporous and Mesoporous Materials*. 77 (2005) 1-45.
- [37] S.K. Das, M.K. Bhunia, A. Bhaumik, *Journal of Solid State Chemistry*. 183 (2010) 1326-1333.
- [38] A.L. Doadrio, E.M.B. Sousa, J.C. Doadrio, J. Pérez Pariente, I. Izquierdo-Barba, M. Vallet-Regí, *J. Controlled Release*. 97 (2004) 125-132.
- [39] H. Yu, Q. Zhai, *Microporous and Mesoporous Materials*. 123 (2009) 298-305.
- [40] R. Mellaerts, K. Houthoofd, K. Elen, H. Chen, M. Van Speybroeck, J. Van Humbeeck, P. Augustijns, J. Mullens, G. Van den Mooter, J.A. Martens, *Microporous and Mesoporous Materials*. 130 (2010) 154-161.
- [41] D. Halamová, M. Badaničová, V. Zelenák, T. Gondová, U. Vainio, *Appl. Surf. Sci.* 256 (2010) 6489-6494.
- [42] S.A. Mirji, S.B. Halligudi, N. Mathew, N.E. Jacob, K.R. Patil, A.B. Gaikwad, *Materials Letters*. 61 (2007) 88-92.
- [43] J. Lee, D. Cho, W. Shim, H. Moon, *Korean Journal of Chemical Engineering*. 21 (2004) 246-251.
- [44] B.L. Newalkar, N.V. Choudary, U.T. Turaga, R.P. Vijayalakshmi, P. Kumar, S. Komarneni, T.S.G. Bhat, *Chemistry of Materials*. 15 (2003) 1474-1479.
- [45] D.F. Evans, H. Wennerström, *The Colloidal Domain: Where Physics, Chemistry, Biology and Technology Meet*, 2nd ed., Wiley-VCH, New York, 1999.
- [46] B. Jönsson, B. Lindman, K. Holmberg, B. Kronberg, *Surfactants and Polymers in Aqueous Solution*, 2: nd ed., John Wiley & Sons, West Sussex, England, 1998.
- [47] I.R. Schmolka, (1973).
- [48] BASF Corporation, 2010.
- [49] P. Alexandridis, J.F. Holzwarth, T.A. Hatton, *Macromolecules*. 27 (1994) 2414-2425.

- [50] E.B. Jorgensen, S. Hvidt, W. Brown, K. Schillen, *Macromolecules*. 30 (1997) 2355-2364.
- [51] G. Wanka, H. Hoffmann, W. Ulbricht, *Macromolecules*. 27 (1994) 4145-4159.
- [52] C. Guo, H.-. Liu, J.-. Chen, *Colloid & Polymer Science*. 277 (1999) 376-381.
- [53] Z. Zhou, B. Chu, *J. Colloid Interface Sci.* 126 (1988) 171-180.
- [54] K. Mortensen, W. Brown, *Macromolecules*. 26 (1993) 4128-4135.
- [55] Y. Su, J. Wang, H. Liu, *The Journal of Physical Chemistry B*. 106 (2002) 11823-11828.
- [56] R.M. Pashley, M.E. Karaman, *Applied Colloid and Surface Chemistry*, Wiley, West Sussex, 2004.
- [57] N.P. Shusharina, S. Balijepalli, H.J.M. Gruenbauer, P. Alexandridis, *Langmuir*. 19 (2003) 4483.
- [58] J.S. Lettow, Y.J. Han, P. Schmidt-Winkel, P. Yang, D. Zhao, G.D. Stucky, J.Y. Ying, *Langmuir*. 16 (2000) 8291-8295.
- [59] A.G. Denkova, E. Mendes, M.-. Coppens, *J. Phys. Chem. B*. 112 (2008) 793-801.
- [60] H. Heerklotz, A. Tsamaloukas, K. Kita-Tokarczyk, P. Strunz, T. Gutberlet, *J. Am. Chem. Soc.* 126 (2004) 16544-16552.
- [61] C. Yu, B. Tian, J. Fan, G.D. Stucky, D. Zhao, *Chem. Comm.* (2001) 2726-2727.
- [62] J. Sun, H. Zhang, M. Ding, Y. Chen, X. Bao, A. Klein-Hoffman, N. Pfänder, D.S. Su, *Chem. Comm.* (2005) 5343-5345.
- [63] H. Zhang, J. Sun, D. Ma, G. Weinberg, D.S. Su, X. Bao, *J. Phys. Chem. B*. 110 (2006) 25908-25915.
- [64] J. Sun, M. Ding, H. Zhang, C. Wang, X. Bao, D.S. Su, A. Klein-Hoffman, G. Weinberg, S. Mann, *J. Mater. Chem.* 16 (2006) 1507-1510.
- [65] P. Alexandridis, J.F. Holzwarth, *Langmuir*. 13 (1997) 6074-6082.
- [66] W.A. Luck, *Top. Curr. Chem.* 64 (1976) 113-180.
- [67] K.D. Collins, M.W. Washabaugh, *Q. Rev. Biophys.* 18 (1985) 323.

- [68] P. Thiyagarajan, D.J. Chaiko, R.P. Hjelm, *Macromolecules*. 28 (1995) 7730-7736.
- [69] R. Kjellander, E. Florin, *J. Chem. Soc. , Faraday Trans. 1*. 77 (1981) 2053.
- [70] E. Florin, R. Kjellander, J.C. Eriksson, *J. Chem. Soc. , Faraday Trans. 1*. 80 (1984) 2889.
- [71] K. Kang, H. Rhee, *Microporous Mesoporous Mater.* 84 (2005) 34-40.
- [72] J.M. Kim, G.D. Stucky, *Chem. Comm.* (2000) 1159-1160.
- [73] P.F. Fulvio, S. Pikus, M. Jaroniec, *J. Colloid Interface Sci.* 287 (2005) 717-720.
- [74] J. Liu, Q. Yang, X.S. Zhao, L. Zhang, *Microporous Mesoporous Mater.* 106 (2007) 62-67.
- [75] C.J. Brinker, *J. Non Cryst. Solids*. 100 (1988) 31-50.
- [76] L.L. Hench, J.K. West, *Chem. Rev.* 90 (1990) 33-72.
- [77] T.N.M. Bernards, M.J. van Bommel, A.H. Boonstra, *J. Non-Cryst. Solids*. 134 (1991) 1-13.
- [78] K. Flodström, C.V. Teixeira, H. Amenitsch, V. Alfredsson, M. Lindén, *Langmuir*. 20 (2004) 4885-4891.
- [79] K. Flodström, H. Wennerström, V. Alfredsson, *Langmuir*. 20 (2004) 680-688.
- [80] A.Y. Khodakov, V.L. Zholobenko, M. Impéror-Clerc, D. Durand, *J. Phys. Chem. B*. 109 (2005) 22780-22790.
- [81] S. Ruthstein, J. Schmidt, E. Kesselman, Y. Telmon, D. Goldfarb, *J. Am. Chem. Soc.* 128 (2006) 3366-3374.
- [82] S. Ruthstein, V. Frydman, D. Goldfarb, *J. Phys. Chem. B*. 108 (2004) 9016-9022.
- [83] N. Gov, I. Borukhov, D. Goldfarb, *Langmuir*. 22 (2006) 605-614.
- [84] P.F. Fulvio, S. Pikus, M. Jaroniec, *J. Mater. Chem.* 15 (2005) 5049-5053.
- [85] Y. Bennadja, P. Beaunier, D. Margolese, A. Davidson, *Microporous Mesoporous Mater.* 44-45 (2001) 147-152.

- [86] A. Galarneau, H. Cambon, F. Di Renzo, F. Fajula, *Langmuir*. 17 (2001) 8328-8335.
- [87] T. Klimova, A. Esquivel, J. Reyes, M. Rubio, X. Bokhimi, J. Aracil, *Microporous and Mesoporous Materials*. 93 (2006) 331-343.
- [88] M. Kruk, L. Cao, *Langmuir*. 23 (2007) 7247-7254.
- [89] F. Kleitz, W. Schmidt, F. Schüth, *Microporous and Mesoporous Materials*. 65 (2003) 1-29.
- [90] F. Bérubé, S. Kaliaguine, *Microporous Mesoporous Mater*. 115 (2008) 469-479.
- [91] B. Tian, X. Liu, C. Yu, F. Gao, Q. Luo, S. Xie, B. Tu, D. Zhao, *Chem. Comm.* (2002) 1186-1187.
- [92] Y.K. Bae, O.H. Han, *Microporous Mesoporous Mater*. 106 (2007) 304-307.
- [93] R. van Grieken, G. Calleja, G.D. Stucky, J.A. Melero, R.A. García, J. Iglesias, *Langmuir*. 19 (2003) 3966-3973.
- [94] D. Margolese, J.A. Melero, S.C. Christiansen, B.F. Chmelka, G.D. Stucky, *Chemistry of Materials*. 12 (2000) 2448-2459.
- [95] R.J.P. Corriu, A. Mehdi, C. Reye, C. Thieuleux, A. Frenkel, A. Gibaud, *New J. Chem.* 28 (2004) 156-160.
- [96] Q. Yang, J. Liu, J. Yang, L. Zhang, Z. Feng, J. Zhang, C. Li, *Microporous and Mesoporous Materials*. 77 (2005) 257-264.
- [97] L.M. Yang, Y.J. Wang, G.S. Luo, Y.Y. Dai, *Microporous Mesoporous Mater*. 81 (2005) 107-114.
- [98] H. Tsai, J.M. Córdoba, E.M. Johansson, M.A. Ballem, M. Odén, *J. Nanosci. Nanotechnol.* (2010) doi: 10.1166/jnn.2010.3609.
- [99] C.-. Yang, B. Zibrowius, W. Schmidt, F. Schuth, *Chem. Mater*. 15 (2003) 3739-3741.
- [100] C.-. Yang, B. Zibrowius, W. Schmidt, F. Schuth, *Chem. Mater*. 16 (2004) 2918-2925.
- [101] H. Cai, D. Zhao, *Microporous Mesoporous Mater*. 118 (2009) 513-517.
- [102] T. Lai, Y. Shu, Y. Lin, W. Chen, C. Wang, *Mater Lett*. 63 (2009) 1693-1695.

- [103] P. Schmidt-Winkel, J. Lukens W.W., D. Zhao, P. Yang, B.F. Chmelka, G.D. Stucky, *J. Am. Chem. Soc.* 121 (1999) 254-255.
- [104] A.L. Doadrio, E.M.B. Sousa, J.C. Doadrio, J. Pérez Pariente, I. Izquierdo-Barba, M. Vallet-Regí, *Journal of Controlled Release.* 97 (2004) 125-132.
- [105] N. Calin, A. Galarneau, T. Cacciaguerra, R. Denoyel, F. Fajula, *Comptes Rendus Chimie.* 13 (2010) 199-206.
- [106] H. Jaladi, A. Katiyar, S.W. Thiel, V.V. Guliants, N.G. Pinto, *Chemical Engineering Science.* 64 (2009) 1474-1479.
- [107] Y. Wang, M. Noguchi, Y. Takahashi, Y. Ohtsuka, *Catalysis Today.* 68 (2001) 3-9.
- [108] J.C. Park, J.H. Lee, P. Kim, J. Yi, in: Sang-Eon Park, Ryong Ryoo, Wha-Seung Ahn, Chul Wee Lee and Jong-San Chang (Ed.), *Studies in Surface Science and Catalysis*, Elsevier, 2003, pp. 109-112.
- [109] X. Cui, J. Ahn, W. Zin, W. Cho, C. Ha, in: Sang-Eon Park, Ryong Ryoo, Wha-Seung Ahn, Chul Wee Lee and Jong-San Chang (Ed.), *Studies in Surface Science and Catalysis*, Elsevier, 2003, pp. 117-120.
- [110] S.K. Jana, R. Nishida, K. Shindo, T. Kugita, S. Namba, *Microporous Mesoporous Mater.* 68 (2004) 133-142.
- [111] W. Zhang, L. Zhang, J. Xiu, Z. Shen, Y. Li, P. Ying, C. Li, *Microporous and Mesoporous Materials.* 89 (2006) 179-185.
- [112] A. Katiyar, S. Yadav, P.G. Smirniotis, N.G. Pinto, *Journal of Chromatography A.* 1122 (2006) 13-20.
- [113] T. Yamada, H. Zhou, K. Asai, I. Honma, *Mater Lett.* 56 (2002) 93-96.
- [114] K. Kosuge, T. Sato, N. Kikukawa, M. Takemori, *Chemistry of Materials.* 16 (2004) 899-905.
- [115] Z. Jin, X. Wand, X. Cui, *Colloids Surf. , A.* 316 (2008) 27-36.
- [116] S. Kubo, K. Kosuge, *Langmuir.* 23 (2007) 11761-11768.
- [117] X. Cui, S. Moon, W. Zin, *Mater Lett.* 60 (2006) 3857-3860.
- [118] N.J. Jain, V.K. Aswal, P.S. Goyal, P. Bahadur, *Colloids Surf. Physicochem. Eng. Aspects.* 173 (2000) 85-94.

- [119] F. Zhang, Y. Yan, H. Yang, Y. Meng, C. Yu, B. Tu, D. Zhao, *J. Phys. Chem. B.* 109 (2005) 8723-8732.
- [120] C. Yu, J. Fan, B. Tian, D. Zhao, G.D. Stucky, *Adv. Mater.* 14 (2002) 1742.
- [121] M. Choi, W. Heo, F. Kleitz, R. Ryoo, *Chem. Comm.* (2003) 1340-1341.
- [122] X. Bao, X.S. Zhao, X. Li, J. Li, *Appl. Surf. Sci.* 237 (2004) 380-386.
- [123] P. Van Der Voort, P.I. Ravikovitch, K.P. De Jong, M. Benjelloun, E. Van Bavel, A.H. Janssen, A.V. Neimark, B.M. Weckhuysen, E.F. Vansant, *J. Phys. Chem. B.* 106 (2002) 5873-5877.
- [124] M. Kruk, M. Jaroniec, S.H. Joo, R. Ryoo, *The Journal of Physical Chemistry B.* 107 (2003) 2205-2213.
- [125] N. Brodie-Linder, G. Dosseh, C. Alba-Simonesco, F. Audonnet, M. Impéror-Clerc, *Mater. Chem. Phys.* 108 (2008) 73-81.
- [126] D. Zhao, J. Sun, Q. Li, G.D. Stucky, *Chem. Mater.* 12 (2000) 275-279.
- [127] M. Chao, H. Lin, H. Sheu, C. Mou, in: A. Sayari and M. Jaroniec (Ed.), *Studies in Surface Science and Catalysis*, Elsevier, 2002, pp. 387-394.
- [128] A. Sayari, B. Han, Y. Yang, *J. Am. Chem. Soc.* 126 (2004) 14348-14349.
- [129] N. Yu, Y. Gong, D. Wu, Y. Sun, Q. Luo, W. Liu, F. Deng, *Microporous and Mesoporous Materials.* 72 (2004) 25-32.
- [130] Y. Wang, F. Zhang, Y. Wang, J. Ren, C. Li, X. Liu, Y. Guo, Y. Guo, G. Lu, *Mater. Chem. Phys.* 115 (2009) 649-655.
- [131] X.Y. Bao, X.S. Zhao, X. Li, P.A. Chia, J. Li, *The Journal of Physical Chemistry B.* 108 (2004) 4684-4689.
- [132] P. Linton, V. Alfredsson, *Chemistry of Materials.* 20 (2008) 2878-2880.
- [133] P. Linton, A.R. Rennie, M. Zackrisson, V. Alfredsson, *Langmuir.* 25 (2009) 4685-4691.
- [134] P. Linton, J.-. Hernandez-Garrido, P.A. Midgley, H. Wennerström, V. Alfredsson, *Phys. Chem. Chem. Phys.* 11 (2009) 10973.
- [135] S. Chen, C. Tang, W. Chuang, J. Lee, Y. Tsai, J.C.C. Chan, C. Lin, Y. Liu, S. Cheng, *Chemistry of Materials.* 20 (2008) 3906-3916.

- [136] Y. Ma, L. Qi, J. Ma, Y. Wu, O. Liu, H. Cheng, *Colloids and Surfaces A: Physicochemical and Engineering Aspects*. 229 (2003) 1-8.
- [137] W.J.J. Stevens, K. Lebeau, M. Mertens, G. VanTendeloo, P. Cool, E.F. Vansant, *J. Phys. Chem. B*. 110 (2006) 9183-9187.
- [138] K. Kosuge, P.S. Singh, *Chemistry of Materials*. 13 (2001) 2476-2482.
- [139] Y. Zhao, J. Zhang, W. Li, C. Zhang, B. Han, *Chem. Comm.* (2009) 2365-2367.
- [140] E.M. Johansson, J.M. Córdoba, M. Odén, *Mater Lett*. 63 (2009) 2129-2131.
- [141] E.M. Johansson, J.M. Córdoba, M. Odén, *Microporous and Mesoporous Materials*. 133 (2010) 66.
- [142] M. Chao, D. Wang, H. Lin, C. Mou, *Journal of Materials Chemistry*. 13 (2003) 2853-2854.
- [143] Y. Fahn, A. Su, P. Shen, *Langmuir*. 21 (2005) 431-436.
- [144] R. Nagarajan, *Polym. Adv. Technol*. 12 (2001) 23-43.
- [145] P.C.A. Alberius, K.L. Frindell, R.C. Hayward, E.J. Kramer, G.D. Stucky, B.F. Chmelka, *Chem. Mater*. 14 (2002) 3284-3294.
- [146] V.V. Guliants, M.A. Carreon, Y.S. Lin, *Journal of Membrane Science*. 235 (2004) 53-72.
- [147] C.J. Brinker, Y. Lu, A. Sellinger, H. Fan, *Adv Mater*. 11 (1999) 579-585.
- [148] D. Grosso, F. Cagnol, G. . . . Soler-Illia, E. . Crepaldi, H. Amenitsch, A. Brunet-Bruneau, A. Bourgeois, C. Sanchez, *Advanced Functional Materials*. 14 (2004) 309-322.
- [149] K. Chao, P. Liu, K. Huang, *Comptes Rendus Chimie*. 8 (2005) 727-739.
- [150] L.C. Huang, E.K. Richman, B.L. Kirsch, S.H. Tolbert, *Microporous and Mesoporous Materials*. 96 (2006) 341-349.
- [151] W. Cho, T. Kim, K. Char, C.L. Soles, *Microporous and Mesoporous Materials*. 131 (2010) 136-140.
- [152] B. Su, X. Lu, Q. Lu, *Langmuir*. 24 (2008) 9695-9699.

- [153] Y. Yamauchi, T. Nagaura, A. Ishikawa, T. Chikyow, S. Inoue, *J. Am. Chem. Soc.* 130 (2008) 10165-10170.
- [154] M. Dutreilh-Colas, M. Yan, P. Labrot, N. Delorme, A. Gibaud, J. Bardeau, *Surf. Sci.* 602 (2008) 829-833.
- [155] R. Pitchumani, W. Li, M. Coppens, in: Abdelhamid Sayari and Mietek Jaroniec (Ed.), *Studies in Surface Science and Catalysis*, Elsevier, 2005, pp. 83-88.
- [156] R. Pitchumani, W. Li, M. Coppens, *Catalysis Today*. 105 (2005) 618-622.
- [157] B. Chen, H. Lin, M. Chao, C. Mou, C. Tang, *Adv. Mater.* 16 (2004) 1657-1661.
- [158] S. Brunauer, P.H. Emmett, T. Teller, *J. Am. Chem. Soc.* 60 (1938) 309-319.
- [159] I. Langmuir, *J. Am. Chem. Soc.* 38 (1916) 2221-2295.
- [160] J. Rouquerol, F. Rouquerol, K.S.W. Sing, *Adsorption by Powders and Porous Solids - Principles, Methodology and Applications*, Academic Press, San Diego, 1999.
- [161] M. Jaroniec, M. Kruk, J.P. Olivier, *Langmuir*. 15 (1999) 5410-5413.
- [162] B.C. Lippens, B.G. Linsen, J.H.d. Boer, *Journal of Catalysis*. 3 (1964) 32-37.
- [163] G. Halsey, *J. Chem. Phys.* 16 (1948) 931-937.
- [164] W.D. Harkins, G. Jura, *J. Am. Chem. Soc.* 66 (1944) 1366-1373.
- [165] E.P. Barrett, L.G. Joyner, P.P. Halenda, *J. Am. Chem. Soc.* 73 (1951) 373-380.
- [166] J.C.P. Broekhoff, J.H. de Boer, *Journal of Catalysis*. 9 (1967) 8-14.
- [167] J.C.P. Broekhoff, J.H. De Boer, *Journal of Catalysis*. 9 (1967) 15-27.
- [168] J.C.P. Broekhoff, J.H. De Boer, *Journal of Catalysis*. 10 (1968) 153-165.
- [169] W.W. Lukens, P. Schmidt-Winkel, D. Zhao, J. Feng, G.D. Stucky, *Langmuir*. 15 (1999) 5403-5409.
- [170] M. Kruk, M. Jaroniec, A. Sayari, *Langmuir*. 13 (1997) 6267-6273.
- [171] M. Jaroniec, L.A. Solocycoc, *Langmuir*. 22 (2006) 6757-6760.
- [172] P.I. Ravikovitch, A.V. Neimark, *Colloids and Surfaces A: Physicochemical and Engineering Aspects*. 187-188 (2001) 11-21.

[173] A.V. Neimark, P.I. Ravikovitch, *Microporous and Mesoporous Materials*. 44-45 (2001) 697-707.

[174] P.I. Ravikovitch, A.V. Neimark, *Langmuir*. 18 (2002) 1550-1560.

[175] S.S. Kim, A. Karkamkar, T.J. Pinnavaia, M. Kruk, M. Jaroniec, *J. Phys. Chem. B*. 105 (2001) 7663-7670.